Decision-making strategies implemented in SolFinder 1.0 to identify eco-efficient aircraft trajectories: application study in AirTraf 3.0

Federica Castino[1], Feijia Yin[1], Volker Grewe[1,2], Hiroshi Yamashita[2], Sigrun Matthes[2], Simone Dietmüller[2], Sabine Baumann[2], Manuel Soler[3], Abolfazl Simorgh[3], Maximilian Mendiguchia Meuser[4], Florian Linke[4], and Benjamin Lührs[4]

[1]Faculty of Aerospace Engineering, Delft University of Technology, Delft, The Netherlands
[2]Institut für Physik der Atmosphäre, Deutsches Zentrum für Luft- und Raumfahrt, Oberpfaffenhofen, Germany
[3]Department of Aerospace Engineering, Universidad Carlos III de Madrid, Madrid, Spain
[4]Lufttransportsysteme, Deutsches Zentrum für Luft- und Raumfahrt, Hamburg, Germany

Correspondence: Federica Castino (f.castino@tudelft.nl)

Abstract.

The optimization of aircraft trajectories involves balancing operating costs and climate impact, which are often conflicting objectives. To achieve compromise optimal solutions, higher-level information such as preferences of decision-makers must be taken into account. This paper introduces the SolFinder 1.0 module, a decision-making tool designed to identify eco-
5 efficient aircraft trajectories, which allow ~~to reduce the~~ the reduction of the flights climate impact with limited cost penalties compared to cost-optimal solutions. SolFinder 1.0 offers flexible decision-making options that allow users to select trade-offs between different objective functions, including fuel use, flight time, NO_x emissions, contrail distance, and climate impact. The module is included in the AirTraf 3.0 submodel, which optimizes trajectories under atmospheric conditions simulated by the ECHAM/MESSy Atmospheric Chemistry model. This paper focuses on the ability of the module to identify eco-efficient
10 trajectories while solving a bi-objective optimization problem that minimizes climate impact and operating costs. SolFinder 1.0 enables users to explore trajectory properties at varying locations of the Pareto fronts without prior knowledge of the problem results and to identify solutions that limit the cost of reducing the climate impact of a single flight.

1 Introduction

Aviation is estimated to contribute ~~to~~ 3-5% of ~~the~~ total anthropogenic global warming (Lee et al., 2021). Aircraft emissions
15 affect the radiative budget of the Earth through several effects, which are usually distinguished between carbon dioxide (CO_2) and non-CO_2 effects (Lee et al., 2010). Non-CO_2 effects account for about 2/3 of the aviation net effective radiative forcing (Lee et al., 2021) and include, among others: the radiative forcing from contrail cirrus (Schumann, 2005; Kärcher, 2018), and the perturbations in the atmospheric concentrations of ozone (O_3) and methane (CH_4) caused by nitrogen oxide (NO_x) emissions (Stevenson et al., 2004; Köhler et al., 2008). The temperature perturbation resulting from CO_2 emissions is only
20 dependent on the amount of emitted CO_2, due to the long atmospheric lifetime of CO_2. To reduce CO_2 emissions, several solutions are currently under development, exploring, for example, the use of new propulsion technologies or alternative

aviation fuels (Staples et al., 2018; Yin and Rao, 2020). Contrarily, non-CO_2 effects occur over short timescales, which typically range from hours (e.g., contrails) to months or years (e.g., NO_x-induced changes on O_3 and CH_4). As a consequence, the temperature perturbation caused by an aircraft unit emission is highly dependent on the time and location of the emission

25 (Köhler et al., 2013; Frömming et al., 2021). Many studies investigated the possibility of using this time and space dependency to reduce the climate effect of a flight, for example, by optimizing its trajectory to minimize the induced temperature increase ~~(Stevenson and Derwent, 2009; Sridhar et al., 2011; Grewe et al., 2017; Matthes et al., 2021; Simorgh et al., 2022).~~ (Stevenson and Derwe . Towards the implementation of this type of operational strategies, some recent studies highlighted the main challenges and opportunities related to the avoidance of climate sensitive regions by aircraft trajectories optimization (Simorgh et al., 2022; Molloy et al., 2

30 . Most importantly, the current level of scientific understanding of the non-CO_2 effects of aviation is lower than the one of CO_2 effects, as demonstrated by the uncertainty ranges of the radiative forcing estimates reported by Lee et al. (2021). Moreover, the identification of climate sensitive regions (e.g., ice-supersaturated regions, supporting persistent contrails) relies on the availability of accurate weather forecast. Depending on the stability of the forecast, trajectories can be optimized via tactical adjustments during the flight or, preferably, in advance (e.g., one day before departure) to limit the associated penalties in

35 operating costs, e.g., minimizing fuel use and workload of flight crew and air traffic controller (Molloy et al., 2022).

Currently, air traffic optimization focuses on minimizing economic penalties, e.g., identifying aircraft trajectories that lead to minimal operating cost. Minimizing the operating cost and the climate impact of a single flight are expected to be conflicting objectives of aircraft trajectory optimization (Yamashita et al., 2021). This implies that, in most cases, it is not possible to identify a solution that simultaneously minimizes both objectives. Therefore, optimizing an aircraft trajectory with respect to

40 its economic cost and climate impact, a set of Pareto-optimal solutions can be identified. To select a single trajectory among this set of optimal solutions, a wide range of decision-making strategies can be employed (Kou et al., 2012; Pasman et al., 2022). In this paper, we present a new decision-making tool, the SolFinder 1.0 module, which was developed with the aim of identifying aircraft trajectories leading to a significant reduction of the flight climate impact, while limiting the increase in economic costs: we define these options as *eco-efficient* aircraft trajectories. This tool satisfies the following requirements: ~~(1)~~

45 – it is applicable to any set of ~~Pareto optimal~~ Pareto-optimal solutions resulting from the optimization of a single aircraft trajectory; ~~(2)~~

– it is suitable for identifying compromise solutions between any number of objective functions; ~~(3)~~

– in particular, when applied for the bi-objective optimization of operating cost and climate impact, it is capable of identifying eco-efficient solutions.

50 To satisfy these requirements, the following options have been selected and are available in the first version of SolFinder: (1) a strategy relying on the VIKOR method (abbreviation from its Serbian name: *Vlse Kriterijumska Optimizacija Kompromisno Resenje*, presented by Opricovic and Tzeng, 2004) to identify eco-efficient solutions; (2) a strategy selecting the Pareto-optimal solution closest to a target percentage change in one of the objectives, such as the economic costs; (3) a decision-making method which combines the previous two options, applying the VIKOR method while limiting the change in one of the objectives. The

55 SolFinder module has been coupled to the ECHAM/MESSy Atmospheric Chemistry (EMAC, Jöckel et al., 2010) submodel AirTraf (Yamashita et al., 2020), as part of the AirTraf extension for the efficient resolution of multi-objective optimization problems. This modelling chain ~~allows~~ enables users to select Pareto-optimal solutions matching specific preferences of decision-makers, e.g., eco-efficient aircraft trajectories, and to explore their dependency on the atmospheric natural variability.

In Sect. 2, we describe the modelling chain, and we present the decision-making strategies included in SolFinder 1.0 (Sect.
60 2.3). In Sect. 3, we illustrate an example application of the selected decision-making strategies, using the Pareto-optimal solutions that are identified by AirTraf when a European air traffic sample of 100 night-time flights is optimized with respect to economic cost and climate impact. In Sect. 4, we compare our results to those obtained in previous studies, and we discuss uncertainties affecting our results. Our key messages are summarized in Sect. 5.

2 Methods

65 We conduct our simulations using the ECHAM/MESSy Atmospheric Chemistry (EMAC) model (Jöckel et al., 2010). This is a numerical climate model system that includes sub-models describing tropospheric and middle atmosphere processes and their interaction with oceans, land and human influences (Jöckel et al., 2010). This system relies on the second version of the Modular Earth Submodel System (MESSy2) to connect multi-institutional computer codes, while the core atmospheric model is the 5th generation European Centre Hamburg general circulation model (ECHAM5, Roeckner et al., 2006). Fig. 1 illustrates
70 the relation between the EMAC model and the three submodels that have a major relevance in our experiments: CONTRAIL (Frömming et al., 2014), ACCF (Yin et al., 2023), and AirTraf (Yamashita et al., 2020).

The EMAC model provides the atmospheric conditions at a specific time and location (e.g., wind, temperature, potential vorticity, relative humidity) to determine the fuel consumption, emission indexes, and climate effects of aircraft emissions. The CONTRAIL submodel computes the potential contrail coverage~~(determination of persistent contrails formation), which is~~
75 ~~used as input for the ACCF and AirTraf submodels~~, i.e., the fraction of the model grid-box where persistent contrails can exist (Burkhardt et al., 2008). The ACCF submodel employs the algorithmic Climate Change Functions (aCCFs) in order to deliver the estimated spatially and temporally resolved climate effect of aviation emissions to AirTraf; lastly, the AirTraf submodel identifies the optimal aircraft trajectories with respect to the routing strategy selected by the user. The optimization process is performed in two steps: (1) a genetic algorithm - Adaptive Range Multi-Objective Genetic Algorithms (ARMOGA, Sasaki and
80 Obayashi, 2005) - is employed to solve a single- or multi-objective optimization problem; (2) if a multi-objective optimization is solved, it is possible that more than one optimal solution is found, thus a decision-making module (SolFinder) intervenes to select a single recommended trajectory, based on the preferences of the user.

2.1 Base model configuration

For the present study, we applied EMAC (ECHAM5 version 5.3.02, MESSy version ~~2.54~~2.55.0) in the T42L31ECMWF-
85 resolution. This resolution has a spherical truncation of T42 (corresponding to a quadratic Gaussian grid of approximately 2.8 by 2.8 degrees in latitude and longitude), and includes 31 vertical hybrid pressure levels up to 10 hPa (i.e., to an altitude
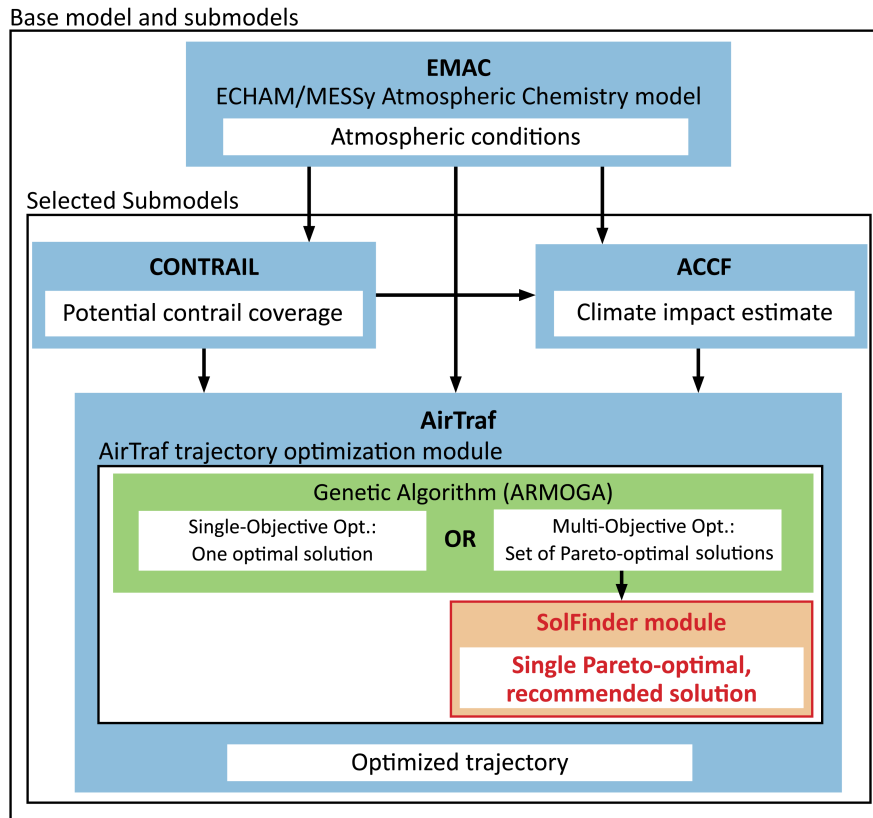
Figure 1. Overview of the relations between EMAC and the three submodels CONTRAIL, ACCF, and AirTraf. The present study focuses on the description of the decision-making module SolFinder 1.0, which is highlighted in red in the diagram.

of approximately 30 km). We describe the model output obtained by simulating the atmospheric conditions occurring from 1 January 2018 to 31 January 2018, employing a temporal resolution of 12 minutes, ~~and nudging~~. To obtain weather conditions aligned with those observed in January 2018, the simulations are conducted nudging by Newtonian relaxation the prognostics variables divergence, vorticity, temperature and the (logarithm of the) surface pressure down to the surface towards the respective ECMWF ERA-Interim reanalysis data (Dee et al., 2011; Jöckel et al., 2016).

2.2 AirTraf submodel

The air traffic simulator AirTraf is responsible for the optimization of the aircraft trajectories, according to the routing strategy prescribed by the user. The submodel requires as input information ~~on~~ (1) the atmospheric conditions at the time and location of the flight, provided by the EMAC model, and ~~on~~ (2) the air traffic sample, including the location of the airports of departure and arrival, the departure time of each flight, and characteristics of the aircraft and engine type to be simulated (Yamashita et al., 2016). Once this information is collected, the genetic algorithm (ARMOGA, Sasaki and Obayashi, 2005) intervenes

to identify an optimal trajectory. The number of design variables of the optimization problem is fixed to 11, since the model describes each aircraft trajectory as a B-spline curve defined by three control points on the horizontal domain (three pairs of coordinates) and five on the vertical cross-section (as illustrated in Yamashita et al., 2016, Fig.6). The domains of the horizontal control points are centered on the great circle connecting the airports of departure and arrival, while the vertical control points are bounded by the flight levels at 29000 ft (FL290) and at 41000 ft (FL410), corresponding to altitudes of about 8.8-12.5 km. To calculate the flight properties along a candidate trajectory, the path is divided in flight segments by $n_{\mathrm{wp}} = 101$ waypoints. In particular, to calculate the fuel used at each flight segment, AirTraf uses the aircraft performance model of Eurocontrol's Base of Aircraft Data (BADA Revision 3.9, Eurocontrol, 2011) and the Deutsches Zentrum für Luft- und Raumfahrt (DLR) fuel flow method (Yamashita et al., 2016).

The version AirTraf 2.0 presented by Yamashita et al. (2020) allowed the user to solve single-objective optimization problems, minimizing one of several available objective functions, including fuel use, flight time, NO_x emissions, contrail distance, operating costs, and climate impact. ~~AirTraf~~ The submodel is being expanded to use the same optimization method for the efficient resolution of multi-objective optimization problems. As a result, it is possible to simultaneously optimize two or more objective functions, without combining such functions into a single objective. This is particularly convenient when we aim to identify eco-efficient aircraft trajectories under a large number of weather conditions. In ~~facts~~fact, a conversion factor would be necessary to combine climate impact and operating costs into a single objective functions. However, this factor (e.g., as defined by Simorgh et al. (2023), Eq.7) is affected by a large variability over different flights and days, thus it is difficult to find a general value of the factor which can be applicable to optimize large air traffic samples over long-term simulations. Due to this AirTraf expansion for the resolution of multi-objective optimization problems, a decision-making module became necessary to ensure that a single optimal solution is identified, and its properties are evaluated and stored by the model. This task can be performed by the SolFinder 1.0 module presented in this paper. Therefore, SolFinder has been coupled to AirTraf to select one optimal solution from the full Pareto set, reducing the computational effort of the model.

In the development of the decision-making strategies implemented in SolFinder 1.0, the underlying goal has been to find eco-efficient aircraft trajectories, compromising between the optimization of climate impact and operating costs. Hence, we include here the definitions of these objective functions within AirTraf. The economic costs of the flights are represented by the Simple Operating Costs (SOC), defined as in Eq. (1):

$$\mathrm{SOC} = c_t \sum_{i=1}^{n_{wp}-1} \mathrm{TIME}_i + c_f \sum_{i=1}^{n_{wp}-1} \mathrm{FUEL}_i \tag{1}$$

where TIME_i and FUEL_i represent the flight time and fuel used at the ith flight segment, respectively, while $c_t = 0.75\ \$/s$ and $c_f = 0.51\ \$/kg$ are the unit time and unit fuel costs (Burris, 2015; Yamashita et al., 2020). The climate impact of each aircraft trajectory is measured in terms of Average Temperature Response over 20 years (ATR20), as provided by the ACCF submodel (van Manen and Grewe, 2019; Yin et al., 2023). The total climate impact $\mathrm{ATR20}_{\mathrm{tot}}$ of each aircraft trajectory is determined summing the contribution from the main climate effects:

$$\text{ATR20}_{\text{tot}} = \sum_{i=1}^{n_{wp}-1} \left[\text{ATR20}_{\text{CO}_2,i} + \text{ATR20}_{\text{H}_2\text{O},i} + \text{ATR20}_{\text{NO}_x\text{-O}_3,i} + \text{ATR20}_{\text{NO}_x\text{-CH}_4,i} + \text{ATR20}_{\text{contrails},i} \right] \tag{2}$$

where each addend represents, from left to right, the ATR20 at the ith flight segment from (1) carbon dioxide (CO_2), (2) water vapour (H_2O), (3) ozone (O_3) from emission of NO_x, (4) methane (CH_4) from emission of NO_x, and (5) contrails. The term $\text{ATR20}_{\text{NO}_x\text{-CH}_4,i}$ includes the changes in primary mode ozone induced by the reduced CH_4 atmospheric concentration, while it neglects the feedback from stratospheric water vapour (Yin et al., 2023). The present study uses ATR20 as climate metric, assuming a business-as-usual Future emission scenario (F-ATR20). Alternative climate metrics can also be used, e.g, considering a time horizon of 100 years (ATR100). A detailed description of the climate metric conversion is presented in ~~Dietmüller et al. (2022)~~Dietmüller et al. (2023).

2.3 SolFinder module

In this section, we describe the decision-making strategies implemented in SolFinder 1.0. Our aim is to solve a multi-objective optimization problem minimizing a set of N objective functions f_n, with $n = 1, 2, ..., N$. If two or more objective functions are conflicting, a set of ~~Pareto optimal~~ Pareto-optimal solutions, P, is identified. The values $f_{n,j}$ of the objective functions are assigned to each Pareto-optimal solution $p_j \in P$, with $j = 1, 2, ..., J$. Subsequently, a decision-making strategy intervenes, to select one solution $p_{\text{rec}} \in P$ which is the *recommended* solution according to the decision-maker criteria. We include the following strategies towards the resolution of our problem: (1) option selecting a solution based on its weighted distance from an ideal (usually, not feasible) solution (VIKOR method, Sect. A) for the identification of eco-efficient trajectories (Sect. 2.3.1); (2) option leading to a target percentage change in one of the objective functions, with respect to its minimum value (Sect. 2.3.2); (3) option combining the previous two strategies, limiting the change in one of the objective functions while applying the VIKOR method (Sect. 2.3.3); (4) selection of one of the extremes of the Pareto-optimal set (Sect. 2.3.4).

A large variety of multi-criteria decision-making methods is currently available to select one solution among a set of optimal options (Wang and Rangaiah, 2017; Sałabun et al., 2020). In a preliminary phase of our research, we considered different options among the most popular techniques, including GRA (Grey Relational Analysis, Wang and Rangaiah, 2017), TOPSIS (Technique for Order Preference by Similarity to Ideal Solution, Chen and Hwang, 1992), and VIKOR (abbreviation from its Serbian name: *Vlse Kriterijumska Optimizacija Kompromisno Resenje*, Sect. A). These options have been implemented in a python library[1], in order to apply them on test cases, and compare their effectiveness in identifying eco-efficient aircraft trajectories. We identified the VIKOR method (Opricovic, 1998; Opricovic and Tzeng, 2004) as a suitable candidate to translate our definition of eco-efficient solutions into a decision-making algorithm. This is due to its peculiarity of recommending more than one solution, if certain criteria are not met by a single solution (Sect. A). This allows ~~to flexibly identify~~ flexible identification of a region of the Pareto-front (e.g., the section of the Pareto-front leading to a small change in the economic costs), within which the ~~decision maker~~ is able to choose their preferred solution (e.g., the solution with the largest climate

---

[1] See Supplement material and (Castino, 2023).

impact reduction). Moreover, no *a priori* knowledge on the optimization problem expected results is needed. To apply the VIKOR method, only the following information is provided as input, translating the user preferences in mathematical terms:

– the relative importance of N objective functions, represented by the weights $w_n \geq 0$, such that $\sum_n w_n = 1$, with $n = 1, 2, ..., N$.

– the relative importance of group utility (preference towards achieving the greatest benefit) and individual regret (preference towards avoiding large penalties), represented by the parameter γ, with $0 < \gamma < 1$. If $\gamma > 0.5$, the *majority rule* principle is applied; contrarily, $\gamma < 0.5$ implies the application of the *veto* principle; lastly, $\gamma \approx 0.5$ represents a *voting by consensus* strategy (Opricovic and Tzeng, 2004).

2.3.1 Strategy using VIKOR method to identify eco-efficient trajectories

The SolFinder 1.0 module identifies eco-efficient trajectories using a decision-making option based on the VIKOR method~~described in~~. This method, introduced by Opricovic (1998) and Opricovic (1998), makes use of the overall distance (group utility) and the maximum distance (individual regret) of a Pareto-optimal solution from the minimal values of the optimization objectives to rank the Pareto-optimal solutions. For more details on the version of the VIKOR method implemented in SolFinder, we refer to Sect. A. Fig. 2 illustrates how this decision-making strategy is applied using as an example the bi-objective optimization of a flight with respect to its SOC and ATR20. Firstly, the decision-making module collects all the Pareto-optimal solutions (represented by the ~~red dots~~ grey crosses in Fig. 2a). Subsequently, the VIKOR method is applied according to the prescribed values of the parameter γ and the relative weights w_n (Fig. 2b). This leads to a recommended subset of optimal solutions (represented by the ~~red dots~~ green triangles in Fig. 2c). If the VIKOR method identifies more than one recommended solution, i.e., the solutions p_v ($v = 1, 2, ..., M$) are equally recommended, the model selects the one with the minimum value of the objective function assigned to the lowest weight w_n. In Fig. 2d, the objective with the lowest relative weight is ATR20 ($w_{\text{ATR20}} = 0.3, w_{\text{SOC}} = 0.7$), thus the model selects the point among the recommended solutions (indicated by the green ~~crosses~~ triangles in Fig. 2d) with the lowest ATR20 (red dot in Fig. 2d).

~~The motivation to this last step in Fig. 2d is due to our goal of identifying~~ This last step is thus formulated to translate in mathematical terms our definition of eco-efficient aircraft trajectories~~. In fact,~~, i.e., a compromise solution between cost-optimal and climate-optimal solutions, such that the largest possible climate impact reduction is achieved, while keeping the operating costs nearly unchanged with respect to the cost-optimal solution. Using the VIKOR method, a subset of Pareto-optimal solutions is identified, according to the relative importance of the two optimization objectives. Therefore, if the highest weight is assigned to the objective function representing operating costs, the VIKOR method equally recommends a subset of Pareto-optimal solutions close to – or, possibly, including - the cost-optimal extreme point of the Pareto-front. Among this subset of equally recommended solutions, we choose the point leading to the largest climate impact reduction, i.e., the minimum value of the objective function assigned to the lowest weight. Therefore, the objective with the highest weight plays a dominant role in the selection of the subset of equally recommended solutions (VIKOR method), while the objective with the lowest weight becomes dominant in the selection of a single solution among this subset.
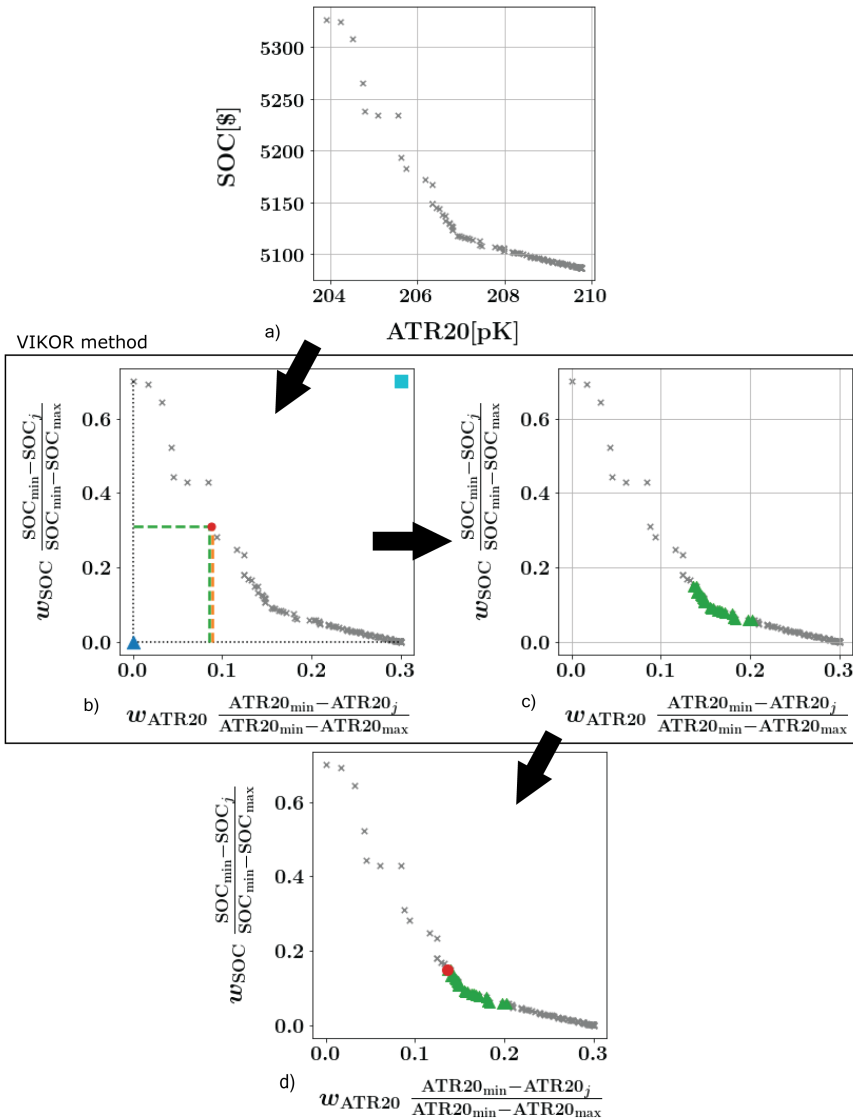
Figure 2. Illustration of the steps performed by the eco-efficient decision-making strategy relying of VIKOR. The aircraft trajectories are optimized to minimize SOC and ATR20, resulting in a set of Pareto-optimal solutions (grey crosses). We set $w_{SOC} = 0.7$, $w_{ATR20} = 0.3$, $\gamma = 0.5$. Panel a) shows the Pareto-optimal solutions (grey crosses) collected before applying the decision-making strategy. Panel b) illustrates the application of the VIKOR method (Sect. A), thus the axes are scaled as in Fig. A1. This step results in the identification of the subset of recommended solutions, represented by the green triangles in panel c). Panel d) shows the selected solution (red dot) among the subset of recommended solutions (green triangles).

The resulting strategy can be configured to follow the ~~following steps~~ steps listed here:

1. A bi-objective optimization problem is solved to simultaneously minimize the total climate impact (ATR20$_{\text{tot}}$ as defined in Eq. (2)) and operating costs (SOC, Eq. (1)). This step results in the identification of J Pareto-optimal solutions (Fig. 2a).

2. The VIKOR method is applied, following the steps described in Sect. A (Fig. 2b).

3. A set of equally recommended solutions are selected in the sections in the Pareto front closest to the cost-optimal solution, by assigning a relatively high weight to the operating costs, i.e., $w_{\text{SOC}} > 0.5$ (with $\gamma = 0.5$). Depending on the shape of the Pareto front, this set of solutions extends towards the best ideal solution, i_{best}, allowing for higher climate impact reductions with respect to the cost-optimal solution, while avoiding cost penalties that are not compensated by a climate impact reduction (Fig. 2c).

4. Among this set of equally recommended solutions, the solution leading to the largest climate impact reduction with respect to the cost-optimal solution is selected, since $w_{\text{ATR}} < w_{\text{SOC}}$. We define this point as the *eco-efficient* solution among the set of ~~Pareto optimal~~ Pareto-optimal options (Fig. 2d).

~~Illustration of the steps performed by the eco-efficient decision-making strategy relying of VIKOR. The aircraft trajectories are optimized to minimize SOC and ATR20, resulting in a set of Pareto-optimal solutions (grey crosses). We set $w_{\text{SOC}} = 0.7$, $w_{\text{ATR20}} = 0.3$, $\gamma = 0.5$. Panel a) shows the Pareto-optimal solutions (red dots) collected before applying the decision-making strategy. Panel b) illustrates the application of the VIKOR method, thus the axes are scaled as in Fig. A1. This step results in the identification of the subset of recommended solutions, represented by the red dots in panel c). Panel d) shows the selected solution (red dot) among the subset of recommended solutions (green crosses).~~

Sensitivity of VIKOR parameterization

To understand the effectiveness the VIKOR method with various configurations of γ and w, we take as example a set of Pareto-optimal solutions, resulting from the bi-objective optimization of an aircraft trajectory with respect to the SOC and ATR20 of the flight. Within this set, a subset of ~~solution~~ solutions is *recommended* by the VIKOR method with different values of γ and $w = [w_{\text{SOC}}, w_{\text{ATR20}}]$. The results of this analysis are shown in Fig. 3. ~~Firstly, we can notice that the~~ This figure illustrates the impact of varying the weights w by comparing different rows. It is possible to see how, increasing the value of w_{SOC} from 0.2 (Fig.s 3a, 3b, 3c) to 0.8 (Fig.s 3j, 3k, 3l), the set of solutions recommended by VIKOR moves closer to the cost-optimal extreme of the Pareto front (0% change in SOC and ATR20). It is less intuitive to understand the impact of changing the parameter γ, which represents the relative importance of group utility. As explained in Sect. 2.3, and according to the formulas included in Sect. A, with $\gamma = 0.5$ the same relative importance is assigned to avoiding large penalties in one of the objectives, and to achieving the greatest overall benefit. In the results presented in Sect. 3.2, we always set the default value $\gamma = 0.5$. A value of $\gamma < 0.5$ leads to the application of the veto principle~~($\gamma < 0.5$,~~, i.e., if one of the objectives is heavily penalized by selecting a certain Pareto-optimal solution, then it will have a low likelihood to be recommended. Therefore, setting $\gamma = 0.25$ (as in Fig.s 3a, 3d, 3g, 3~~l~~j) leads to the exclusion of elements located in the external sections of the Pareto-front~~. When a high value is~~

assigned to ART20 ($w_{\text{ATR20}} = 0.8$), and , because of their distance to the opposite extreme of the Pareto front. On the other hand, when the veto principle is not applied ($\gamma \geq 0.5$), the method selects the section of the Pareto-front including the solution minimising ATR20 (Fig. 3b, 3c). Similarly, set of recommended solutions (green triangles) can include the solution minimising the objective with the highest relative weight. For example, when $w_{\text{SOC}} = 0.8$ and $\gamma \geq 0.5$, the solution with minimum SOC is

230   included in the set of Pareto-optimal solutions (Fig. 3m, 3nk, 3l).
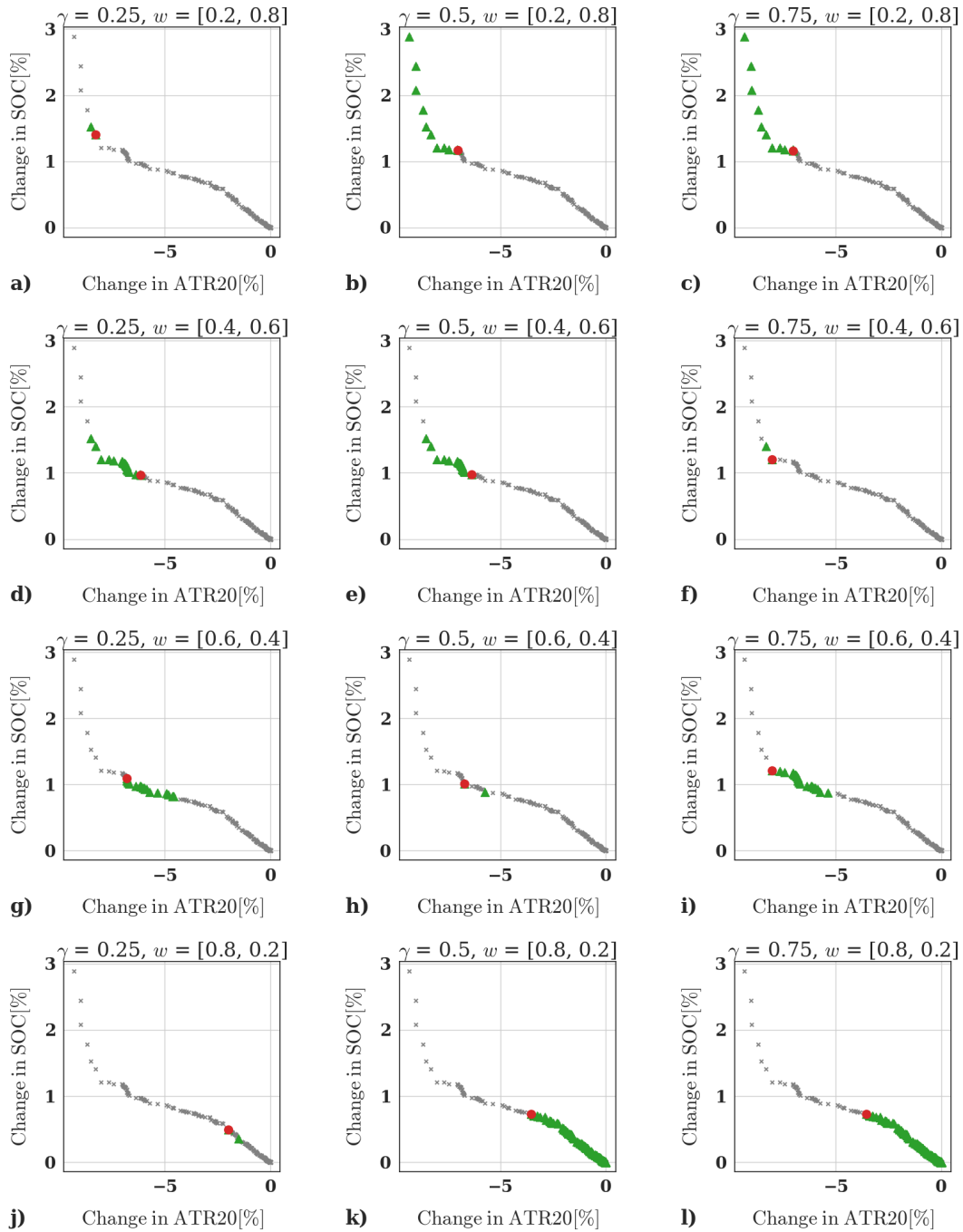
Figure 3. Variability of the selected solution (red dots) using the eco-efficient decision-making method. The grey dots represent the Pareto-optimal solutions, while the green triangles indicate the subset of solutions recommended by the VIKOR method. The axes show percentage changes in the objective functions, relative to the solution minimizing SOC. In this example, the Pareto front consists of 308 solutions.

This observation is the base for the definition of *eco-efficient* solution given at the end of Sect. 2.3.1, i.e., the solution selected with a high relative weight of SOC (w_{SOC} larger than 0.5) and $\gamma = 0.5$. Following this definition, the selected solution shown in Fig. 3~~m~~ k (represented by a red dot) is an eco-efficient solution. In fact, this solution leads to the maximum ATR20$_{tot}$ reduction among the subset of the solutions recommended by VIKOR (green dots), while being equally recommended as the cost-optimal solution by the VIKOR method. In other words, the selected solution in Fig. 3~~m~~ k follows the definition of eco-efficient solutions given in the Introduction, i.e., it allows for a significant reduction in the flight climate impact, while avoiding significant increases in operating costs. However, we note that determining the values of γ and w remains an arbitrary choice, which reflects the specific preferences of the decision-maker. Further elements to consider when setting these parameters are discussed later in Sect. 3.

~~Variability of the selected solution (red dots) using the eco-efficient decision-making method. The grey dots represent the Pareto-optimal solutions, while the green triangles indicate the subset of solutions recommended by the VIKOR method. The axes show percentage changes in the objective functions, relative to the solution minimizing SOC. In this example, the Pareto front consists of 308 solutions.~~

2.3.2 Target percentage change in one of the objective functions

In some scenarios, the ~~decision maker requires~~ decision-maker wishes to limit the penalty of one of the objective functions, e.g., to avoid unsustainable increases in the operating costs. Therefore, in the second decision-making strategy, we propose to select the solution p_{rec} leading to a percentage change in one of the objective functions, f_p. On the other hand, to obtain the expected outcome, this option requires certain information on the optimization results to be known before solving the problem, such as the typical shape of the Pareto fronts, and reference values at their extreme points. The threshold for the allowable change is specified as a target value x_t. This is translated in the following process:

$$f_{p,\text{ref}} = \min_j f_{p,j}, \qquad j = 1, 2, ..., J \tag{3}$$

$$x_j = 100 * \frac{f_{p,j} - f_{p,\text{ref}}}{f_{p,\text{ref}}} \tag{4}$$

$$\Delta x_j = |x_j - x_t| \tag{5}$$

Therefore, the selected Pareto-optimal solution $p_{rec} \in P$ is the solution corresponding to the relative change x_{rec}, such that $\Delta x_{rec} = \min_j \Delta x_j$.

Fig. 4 illustrates which solution is selected within a Pareto-optimal set resulting from the resolution of a tri-objective optimization problem, simultaneously minimizing flight time, fuel use, and ATR20$_{tot}$. In this example, $x_t = +0.5\%$ is set as the target percentage change in flight time.
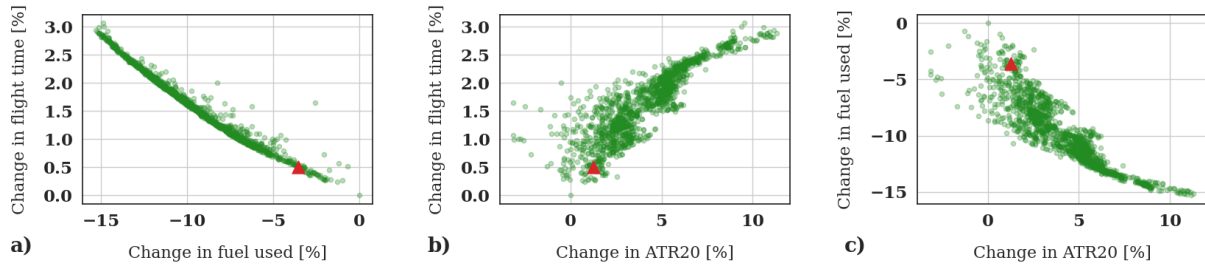
Figure 4. Example of selecting the solution among the Pareto-surface matching a target increase in 0.5% in flight time (indicated by ~~the~~ red ~~cross~~triangles). The green dots indicate the Pareto-optimal solutions, which result from a tri-objective optimization problem minimizing flight time, fuel use, and ATR20$_{\text{tot}}$.

2.3.3 Hybrid option: VIKOR method with target percentage change in one of the objectives

To combine the advantages of the two decision-making strategies presented, a hybrid option is considered, limiting the variability in one of the objective functions while applying the VIKOR method. When this strategy is selected, the decision-maker provides: (1) the configuration of the VIKOR method, setting the parameters γ and w, and (2) a target percentage increase x_t in the objective f_p. Subsequently, the following decision-making process is followed:

1. Apply the VIKOR method and select the recommended solution minimizing the objective function having the lowest weight w_n, as described in Sect. A.

2. Calculate x_p, representing the relative change in f_p of the recommended solution with respect to the minimum value of f_p.

3. If $x_p > x_t$, replace the recommended solution identified in step 1. with the the Pareto-optimal solution leading to a target percentage change x_t in the objective function f_p (in other words, apply the strategy described in Sect. 2.3.2).

This strategy addresses the fact that, with the VIKOR method, no limit in the percentage increase of the objective is set, thus a fraction of the solutions can be affected by changes much larger than the average, as ~~it~~ is shown in a later section of this paper (Sect. 3.2, Fig. 7). With this hybrid option, the VIKOR method can be employed to ~~identified~~ identify eco-efficient trajectories, while introducing a constraint on the operating costs, to prevent increases in the operating costs of some flights that the ~~decision maker~~ decision-maker does not accept.

2.3.4 Selecting one extreme of Pareto-optimal set

Lastly, an additional option is considered to select a solution minimizing one of the objective functions f_n, which we indicate as f_{min}. This simple decision-making process selects the optimal-solution corresponding to the result of a single-objective optimization minimizing f_{min}. Nevertheless, it can be useful to implement this method to identify which values are used as reference during the resolution of the multi-objective optimization problem, and to verify the performance of the model.

3 Application of decision-making method to analyse trajectories' variability along Pareto-front

We now present an example study, in which different settings of the decision-making strategies are compared. This application exemplifies how the decision-making strategies can be employed, and what to consider to determine the settings that best translate the decision-maker preference. In this example, we focus on the suitable settings to identify eco-efficient aircraft trajectories. Nevertheless, SolFinder can also be used to comply with alternative decision-making preferences, by changing the settings of AirTraf and SolFinder.

3.1 Simulations set-up

As previously stated, we intend to identify eco-efficient aircraft trajectories, i.e., trajectories reducing the climate impact at limited changes in the operating costs. Therefore, we solve a bi-objective optimization problem, aiming to simultaneously minimize SOC and ATR20, as defined in Sect. 2.2. We conduct one-month simulations, from 1 January 2018 to 31 January 2018. On each simulation day, 100 night-time flights departing at 00:00 UTC are optimized. Fig. 5 shows the locations of the airports of origin and destination, which were selected considering the Available Seat Kilometres (ASK) for the European Civil Aviation Conference (ECAC) area in 2018 (Matthes et al., 2023a). The same criterion was used to select the A320-214 (CFM56-5B4) as the aircraft/engine type to be simulated. The climate impact of each aircraft trajectory is estimated using the aCCF 1.0A (Matthes et al., 2023b). Table 1 summarizes the model configuration.
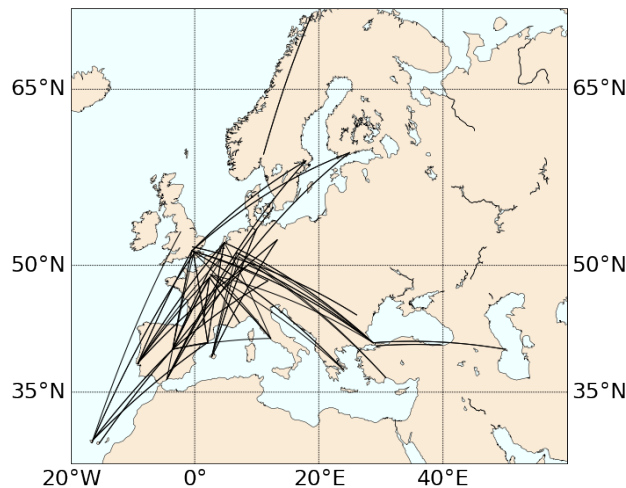
Figure 5. Location of the 100 flights included in the air traffic sample. Each curve represents the great circle connecting an origin/destination pair. Note that most origin/destination pairs are connected by two flights, i.e., one for each direction, thus the number of curves is lower than 100. The list of ICAO airport codes is included in Sect. B.

To compare the effects of using different decision-making strategies, we perform two sets of experiments, whose characteristics are summarized in Table 2, and explained below:

Table 1. Main settings of ECHAM5, ACCF, and AirTraf.

	ECHAM5
Horizontal resolution	T42 (2.81° × 2.81°)
Vertical resolution	L31ECMWF (31 vertical pressure levels up to 10 hPa $\sim$ 30 km)
Time step	12 min
Duration	1-31 Jan. 2018 (each day, 1 month)
	ACCF
Version aCCFs	V1.0A
Climate metric	F-ATR20
Forcing efficacy	Included
	AirTraf
Trajectory waypoints	101
Aircraft / Engine	A320-214 (CFM56-5B4)
Air Traffic Sample	Top 100 routes by ASK for the ECAC area in 2018
Departure time	00:00
Optimization strategy	Multi-objective optimization of: (1) SOC, (2) ATR20$_{tot}$

1. In the first set of experiments, the VIKOR method is employed as we described in Sect. 2.3.1, fixing $\gamma = 0.5$ and varying the relative weight w_{SOC} between 0.2 and 0.9 (Table 2). Therefore, we obtain a total of six selected trade-off solutions. The density of w_{SOC} values increases for higher values of w_{SOC}, as these values lead to the selections of solutions in the section of the Pareto-front of major interest when searching for eco-efficient trajectories, that is, the section closer to the cost-optimal solution. Additionally, we select the two solutions located at the Pareto-front extremes, i.e., the cost-optimal and climate-optimal solutions, with the routine mentioned in Sect. 2.3.4. No preliminary knowledge about the expected problem results is needed to conduct these simulations. As a result of this first set of experiments, for each optimized flight we obtain information on eight solutions that determine the shape and extension of the Pareto-fronts relative to individual flights, and the relation between penalties and benefit aggregated over the whole air traffic sample.

2. In the second set of experiments, we explore the effects of selecting a solution leading to a target change in SOC (Sect. 2.3.2). The target values are chosen using the results form the first set of experiments, which obtained average SOC increases up to about +3.0% (see Table 3 and Fig. 6). In light of these results, we vary x_t from 0.5% to 3.0% (Table 2), selecting four solutions per flight. Moreover, we set $w_{SOC} = 0.7$ to exemplify the effects of using the option of using VIKOR while setting a target SOC change (Sect. 2.3.3) of +1.0%.

Table 2. Overview of the two sets of experiments performed to exemplify the use of the different decision-making methods.

Set	SolFinder strategy	Num. selected sol.	Parameter	Description	Value(s)
1	**VIKOR method for eco-eff.**	6	γ	Group utility weight	0.5
			w_{SOC}	Rel. weight of SOC	0.2, 0.4, 0.6, 0.7, 0.8, 0.9
			w_{ATR}	Rel. weight of ATR20$_{tot}$	$1 - w_{SOC}$
	Pareto-front extremes	2	f_{min}	Minimized objective	ATR20$_{tot}$ or SOC
2	**Target change in f_p**	4	f_p	-	SOC
			x_t	Target change [%]	0.5, 1.0, 2.0, 3.0
	Hybrid VIKOR-target option	1	γ	Group utility weight (VIKOR)	0.5
			w_{SOC}	Rel. weight of SOC (VIKOR)	0.7
			w_{ATR}	Rel. weight of ATR20$_{tot}$ (VIKOR)	$1 - w_{SOC}$
			f_p	objective with limited changes	SOC
			x_t	Limit and target change [%]	1.0

3.2 Results

As explained in Sect. A, one of the main advantages of the VIKOR method is that no knowledge of the expected results is needed before solving our problem. For this reason, the first set of experiments applies the VIKOR method with a range of values of the parameter w_{SOC}. This enables us to perform a preliminary examination of the characteristics of the relation between benefit (in our application, ATR20$_{tot}$ reduction) and penalty (increase in SOC). ~~Relatively~~ Relative to our problem, this relation is shown in Fig. 6, illustrating the change in SOC that is required to achieve a certain reduction in ATR20. The grey curves in Fig. 6b are obtained aggregating the 100 Pareto-optimal solutions selected using the VIKOR method on each simulation day, varying the relative weight w_{SOC} of the objective function SOC. The coordinates of the points connected by the black line (representing the average relation over the 31 simulated days) can be found in Table 3. Setting a low value of w_{SOC} (e.g., $w_{SOC} = 0.2$), we obtain a reduction in ATR20$_{tot}$ of about 13%, which is almost as large as the maximum potential reduction achieved selecting a climate-optimal routing strategy. Moving along the curve towards the cost-optimal strategy, the

magnitude of the ATR20$_{tot}$ reduction decreases. This occurs with a simultaneous decrease of the cost per Kelvin reduction in climate impact, measured by the climate-cost coefficient k [\$/K] (Table 3). This coefficient is defined as (Matthes et al., 2017):

$$k = \frac{\text{SOC} - \text{SOC}_{\text{cost-opt}}}{\text{ATR20}_{\text{cost-opt}} - \text{ATR20}} \tag{6}$$

where ATR20$_{\text{cost-opt}}$ and SOC$_{\text{cost-opt}}$ are relative to the cost-optimal solution, while ATR20 and SOC are relative to the considered decision-making strategy. From this first set of experiments, we understand that: (1) the average ΔATR20$_{tot}$ ranges from -3.5 to -14.4%, with an increase in SOC of 0.1-3.0%, respectively; (2) about half of the maximum feasible climate change reduction can be achieved with only +0.5% in SOC.
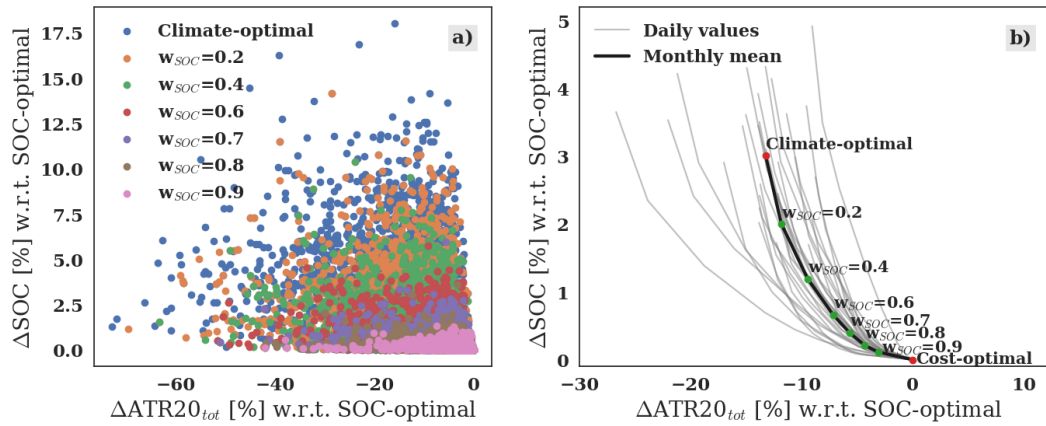
Figure 6. Relation between the relative changes in climate impact, ΔATR20$_{tot}$ [%], and in simple operating cost, ΔSOC [%], with respect to the cost-optimal solution. ~~The~~ *Panel a):* scatter graph of ΔATR20$_{tot}$ [%] against ΔSOC [%], comparing the values ~~are~~ obtained varying the weight of simple operating costs w_{SOC}. *Panel b):* values obtained summing over the 100 routes optimized per day. The black line illustrates the average values over the 31 days included in the simulations, connecting the points selected varying the VIKOR weight w_{SOC} from 0.2 to 0.9 (green dots). The extremes of the Pareto fronts (climate- and cost-optimal solutions, red dots) are included. The gray lines represent the Pareto fronts obtained on each simulation day.

As previously mentioned, the red and green points highlighted in Fig. 6b result from summing all the solutions selected for the 100 flights, and averaging over the month of simulation. However, each optimized trajectory is characterised by a different change in ATR20$_{tot}$ and SOC with respect to its corresponding cost-optimal solution. We note here that this cost-optimal solution (shown in red in Fig. 6b), which we take as reference to calculate the relative changes in ATR20$_{tot}$ and SOC, is specific to each route and each simulation day, thus it varies between different flights. The full variability of the relationship between relative changes in ATR20$_{tot}$ and SOC is illustrated in Fig. 6a. In this panel, one can see that specific solutions can show large deviations from the average values, as some solutions reach an absolute ΔATR20$_{tot}$ larger than 60% at penalties lower than 2.5% in terms of ΔSOC. Moreover, Fig. 6a shows that the subsets of Pareto-optimal solutions obtained setting different w_{SOC} behave as expected: moving to higher values of w_{SOC} leads to subsets that are confined below lower increases

in SOC, while they still stretch towards high ATR20$_{tot}$ reductions (e.g., see the points selected with w_{SOC}=0.9, highlighted in pink). The distributions of ΔATR20$_{tot}$ and ΔSOC values across the optimized flights are represented in Fig. 7, which compares

340   the results obtained varying the parameter w_{SOC} applying the VIKOR method, and the climate-optimal scenario. Fig. 7b shows the percentage of flights characterized by a certain ΔSOC. One can see that, employing VIKOR, the mode of each curve is close to ΔSOC $\sim$ 0%, while the mean and maximum ΔSOC values increase when the weight w_{SOC} decreases. Looking at the ΔATR20$_{tot}$ distributions in Fig. 7a, we can observe larger differences also in the modal values for varying w_{SOC}.
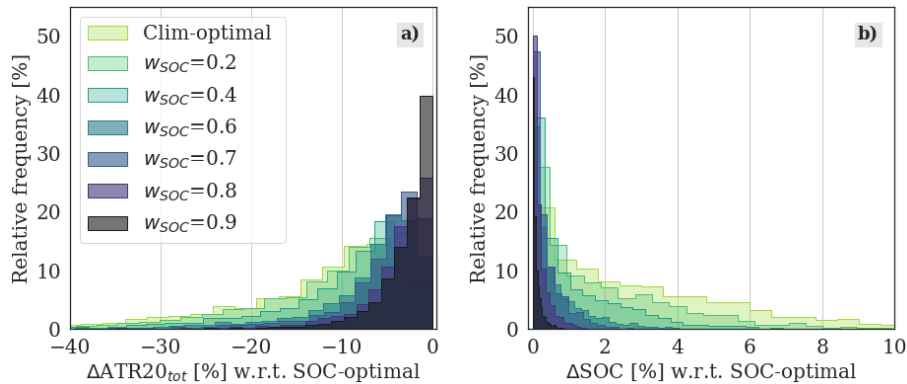
Figure 7. Relative frequencies [%] of different values of ΔATR20$_{tot}$ [%] (Fig. 7a), and of ΔSOC [%] (Fig. 7b) with respect to the cost-optimal solution. The histograms compare the distributions of the values obtained with different decision-making strategies, considering the 100 flights optimized on each simulation day (31*100 values per histogram). The solutions are selected by identifying the minimum climate impact (climate-optimal solutions), or employing the VIKOR method with varying w_{SOC} (first set of experiments).

The results of the first set of experiments can then be used to conduct the second set, fixing a target or a limit increase in

345   SOC as described in Sect. 3.1. The result of this second set of experiments are shown in Table 4. To illustrate the difference of employing different decision-making methods, it is useful to compare Fig. 7 with Fig. 8. The most evident difference emerges comparing Fig. 7b with Fig. 8b. As intended, when we set a target increase in SOC (e.g., +1.0%), most of the selected flights are affected by an increase in SOC equal or similar to the target, thus the curves are centered on this ΔSOC value. However, we can also deduce that some ~~Pareto-front~~ Pareto-fronts do not extend to the target ΔSOC, since values of ΔSOC which are lower

350   than the target are assigned to a fraction of the flights. This results in average ΔSOC values that are lower than the targets, as we can see in Table 4. For example, a total increase of 0.8% in SOC is obtained, when the target is set to 1.0%. Moreover, Fig. 8b shows what distribution of ΔSOC the user can expect employing the hybrid method described in Sect. 2.3.3. The histogram relative to the hybrid option (yellow, hatch-filled) corresponds to the one obtained with VIKOR (with w_{SOC}=0.7), with an additional peak at the determined target SOC increase (1.0%), replacing the larger SOC increases observed in Fig.

355   7b. The results illustrated in Figs. 7b and 8b confirm that the strategies available in SolFinder 1.0 are correctly implemented, and lead to the expected selection of Pareto-optimal solutions. Moreover, the possibility of relying on the VIKOR method to identify eco-efficient trajectories is confirmed by Fig. 9. These curves represent the distributions of the climate-cost coefficient

k [$/K], obtained using VIKOR (blue curves) or the target SOC change (red curves). It is possible to observe that lower values of k are obtained using VIKOR, in particular when a relatively high weight is assigned to SOC.
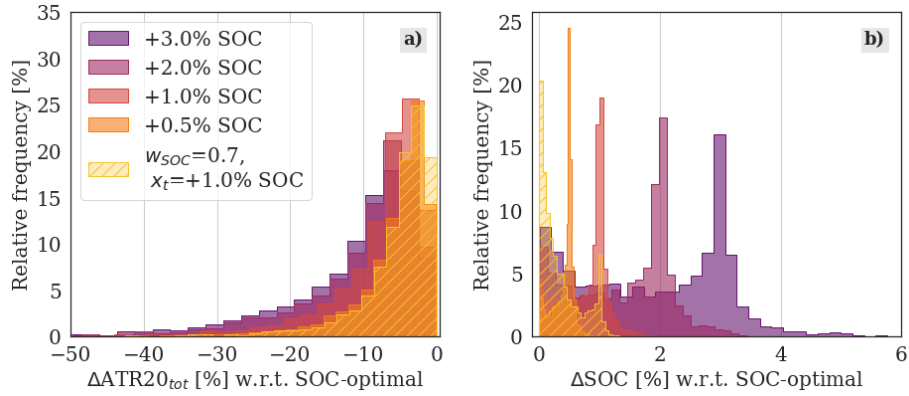
Figure 8. Relative frequencies [%] of different values of $\Delta\text{ATR20}_{\text{tot}}$ [%] (Fig. 8a), and of ΔSOC [%] (Fig. 8b) with respect to the cost-optimal solution. The histograms compare the distributions of the values obtained with different decision-making strategies, considering the 100 flights optimized on each simulation day (31*100 values per histogram). The solutions are selected by targeting different SOC changes, or applying the hybrid method with w_{SOC}=0.7 and $x_t = 1.0\%$ (second set of experiments).
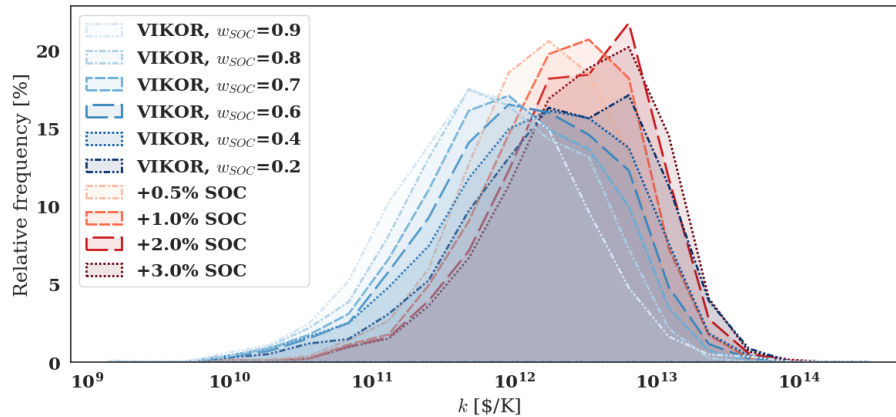
Figure 9. Relative frequencies [%] of different values of the climate-cost coefficient k [$/K], comparing the SolFinder solution-picking strategies using VIKOR (blue curves) or the target SOC change (red curves). The curves approximate the histogram outlines (connecting the bars centers) to highlight the shapes of the distributions and facilitate their comparison. Each curve includes the values obtained with different decision-making strategies, considering the 100 flights optimized on each simulation day (31*100 values per histogram).

360   Employing different decision-making strategies, we obtain trajectories which are characterized by different properties. How these properties vary is shown in Fig. 10, which compares the mean flight altitudes and flown distances obtained when different decision-making strategies are selected. Firstly, we can notice that cost-optimal flights are characterized by the highest mean

flight altitudes and the shortest trajectories ~~, to minimize fuel consumption~~ among the solutions considered, due to the presence of fuel consumption in the optimization objective. On the opposite situation, the lowest altitude and the longest distances

365 are obtained for climate-optimized flights. This confirms previous studies, which commented that (1) aircraft emissions have lower climate impact at lower altitudes, e.g., due to shorter residence time of emitted species (Castino et al., 2021; Matthes et al., 2021; Frömming et al., 2012), and (2) lateral deviations may be necessary to avoid climate sensitive regions (Matthes et al., 2020). Moreover, the variability of the flight properties across the set of simulated flights is larger for climate-optimized flights than for cost-optimal ones. For example, comparing the different variability in flight altitudes, we see the impact of

370 the lowest aerodynamic drag, which ~~allow to minimize~~ allows minimal fuel use, is systematically found at higher altitudes. Contrarily, the altitude leading to the minimal ATR20 is highly variable, due to the high temporal and spatial variability of the atmospheric conditions determining the net flight ATR20. Trade-off solutions between these two extreme scenarios show intermediate properties, with median values and interval bars which gradually evolve moving from one extreme of the curve in Fig. 6 to the other. We can also see that employing the VIKOR method rather than fixing a target increase in costs can lead to

375 different tendencies in the average characteristics of the selected trajectories. For example, comparing the VIKOR method with $w = 0.4$ (causing ΔSOC $\sim +1.2\%$, see Table 3) and setting a target $+1.0\%$ change in SOC, we can see that the latter strategy leads to a less frequent selection of lower flight altitudes, while flying longer trajectories, than the former case. Therefore, the user is recommended to identify their preferred decision-making strategy by also considering these secondary aspects, and not exclusively the resulting distributions in objective functions values.

380 Lastly, we analyse the contribution to the total change in ATR20 of each effect of aviation emissions that we considered in our optimization process: CO_2, H_2O, contrails, NO_x via perturbation of ozone, and NO_x via methane depletion. The relative importance of these effects under different decision-making strategies is illustrated in Fig. 11.

~~Contribution of different climate effects of aviation to the absolute ΔATR20 Kwhen employing different decision-making strategies. The horizontal, dotted line distinguish between solutions selected using VIKOR or climate-optimal solutions (upper~~

385 ~~section), solutions selected targeting a SOC relative change (middle section), and solutions selected applying the hybrid method (lowest bar). The vertical, dashed line separates positive (warming) from negative (cooling) values of ΔATR20.~~

Firstly, we can notice that the ATR20 from CO_2 emissions increases moving from cost-optimal to climate-optimal and compromise solutions. This increase is expected, as the climate impact of CO_2 is independent ~~from~~ of the background atmospheric conditions at time and location of emission; thus it is simply proportional to the amount of fuel used, which is minimized by

390 cost-optimal flights. On the other hand, the increase in the ATR20 from CO_2 is largely compensated by the reduction in the ATR20 from contrails and, secondarily, from the impact of NO_x on ozone. Moreover, Fig. 11 shows that reduction in climate impact of contrails becomes increasingly dominant over the reduction of the other effects, when the relative weight w_{SOC} of SOC increases. This aspect should be considered when selecting the preferred settings of the ~~decision making~~ decision-making strategy. For example, if the decision-maker is interested in reducing both the climate impact of contrails and NO_x-ozone

395 via trajectory optimization, this goal can be achieved allowing larger changes in SOC than those needed to only reduce the ATR20 from contrails effects. The dominant contributions of contrails and, secondarily, of the NO_x climate impact to the ATR20 reduction is confirmed by the results obtained optimizing aircraft trajectories with different tools (Lührs et al., 2021;
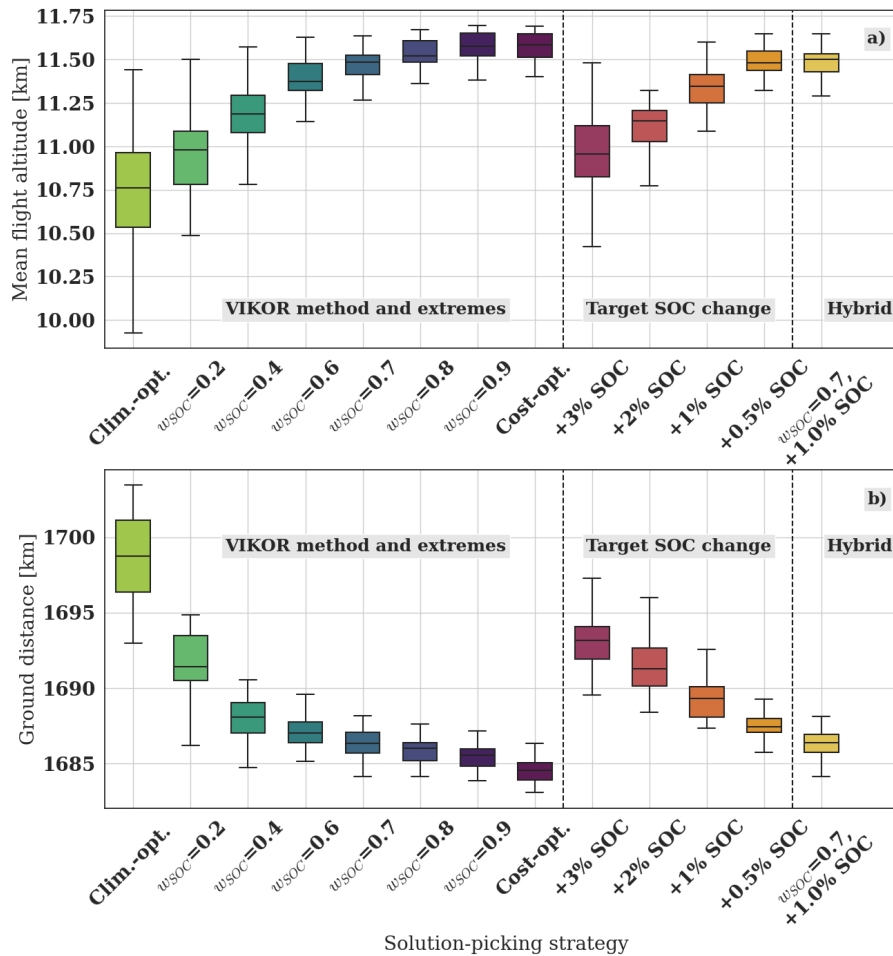
Figure 10. Variability of mean flight altitudes [km] (Fig. 10a) and ~~flown~~ ground distance [km] (Fig. 10b) when employing different decision-making strategies. The flight altitudes are calculated averaging over each trajectory, and over the 100 flights optimized on each day. The ~~flown~~ ground distances represent the total length of each trajectory, averaged over the 100 flights optimized on each simulation day. The boxes extend between 1st and 3rd quartiles over time, and include segments marking the median values. The whiskers indicate the the distribution of the remaining values (excluding eventual outliers).

Simorgh et al., 2022). However, large uncertainties affect the estimates of non-CO_2 effects of aviation (see Sect. 1 and 4), which can heavily affect the relative importance of the different effects of aviation emissions. Therefore, it is relevant to update the modelling chain presented here when enhancements in the scientific understanding and in our ability to model non-CO_2 effects are available, for example, via updated aCCFs versions.

400
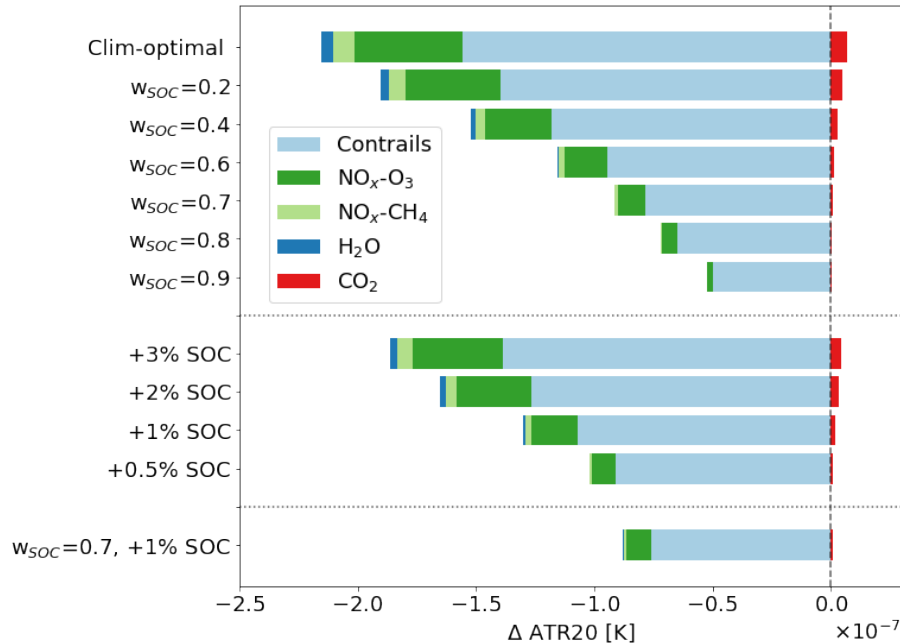
Figure 11. Contribution of different climate effects of aviation to the absolute ΔATR20 [K] when employing different decision-making strategies. The horizontal, dotted line distinguish between solutions selected using VIKOR or climate-optimal solutions (upper section), solutions selected targeting a SOC relative change (middle section), and solutions selected applying the hybrid method (lowest bar). The vertical, dashed line separates positive (warming) from negative (cooling) values of ΔATR20.

4 Discussion

In this paper, we illustrated the ~~decision making~~ decision-making strategies implemented in the SolFinder 1.0 module, and how they can be used to identify eco-efficient trajectories. The climate-optimization of aircraft trajectories has been increasingly

405 researched in the last decade, as efforts to reduce the climate impact of aviation lead to the investigation of operational mitigation strategies. For example, Grewe et al. (2017) optimized a set of transatlantic flights during eight representative weather patterns in winter and summer, employing the air traffic simulator SAAM and the Climate Change Functions (CCFs). This study found that a 10% reduction in climate impact can be achieved with a 1.0% increase in operating costs~~allows to reduce the climate impact by 10%~~. In our study, we considered a different region of the airspace (European flights), and we in-

410 cluded a larger number of weather patterns (every day in the month of January 2018), but limited to the winter season and to night-time; nevertheless, we found the results in Grewe et al. (2017) to be aligned with those we presented in Sect. 3, since a ΔSOC $\sim +1.2\%$ corresponds to a ΔATR20 $\sim -10.3\%$ (Table 3). The maximum feasible climate impact reduction is higher (about 20%) in Grewe et al. (2017), but this is achieved with an approximately double increase in costs. The discrepancy in the section of the Pareto-front closer to the climate-optimal solution may be due to the different temporal and spatial domains.

415 The mitigation potential of optimized aircraft trajectories is expected to be affected by seasonal and daily variability (e.g.,

Reutter et al. (2020); Castino et al. (2021)), thus the methodology presented in this paper can be extended to cover multiple years, to investigate this aspect. Under specific weather conditions, cost-benefit relations were found to show higher eco-efficiency than ~~what we~~ were found aggregating the model output over all the routes, and all the simulated days. For example, Lührs et al. (2021) analysed a day characterised by a weather situation with strong contrail formation, and found that a 0.75% increase in fuel used halved the climate impact. This study suggests the possibility of identifying weather situations that allow for a higher eco-efficiency than others. The modelling chain presented in this paper enables us to optimize aircraft trajectories under a large number of different atmospheric conditions, within a feasible computational time. Therefore, on-going research is using the newly developed version of AirTraf, coupled with the SolFinder module, to analyse under which weather conditions eco-efficient aircraft trajectories are most likely to be identified. To this end, additional decision-making strategies are being investigated, to exploit the ability of VIKOR to identify lower values of the climate-cost coefficient k than a strategy applying a target increase in SOC to all flights (Fig. 9). Two candidate additional strategies are illustrated in Fig. 12. With these options, only a fraction of the flights identified by VIKOR is climate-optimized, due to an additional condition. This is obtained setting a threshold value of the coefficient k, in order to climate-optimize only the top ranked half of the flights (Fig. 12a) or until a certain budget is spent (e.g, +0.5% of SOC in Fig. 12b). A disadvantage of these decision-making strategies is that their settings configuration relies on information on the whole system of optimized flights, which is not available when we consider the Pareto front resulting from a single-flight optimization. Therefore, preliminary simulations have to be run to derive some parameter values, for example the specific threshold value of the climate-cost coefficient k [\$/K]. Because of the large variability of k, these decision-making strategies are more reliant on the results obtained from previous simulations than the strategies included in SolFinder 1.0.
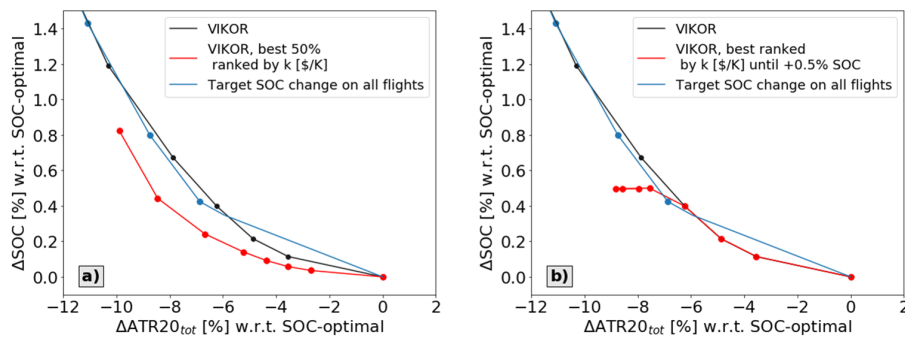
Figure 12. Relation between the percentage changes in climate impact, ΔATR20 [%], and in simple operating cost, ΔSOC [%], with respect to the cost-optimal solution. The values are obtained aggregating the properties of all the optimized flights (31 days, 100 routes optimized per day). The black curve connects the points obtained with the SolFinder strategy relying on VIKOR, while the blue line and points refer to the SolFinder strategy targeting a fixed SOC change. The red lines refer to additional strategies considered for future versions of SolFinder: optimization of the 50% of the flights best ranked by k (Fig. 12a), and optimization of the flights best ranked by k until an increase in SOC of 0.5% is achieved.

The present work estimates the climate effect of aviation resulting from the emission of CO_2, H_2O, NO_x, and from the formation of contrail-cirrus. Estimating the radiative forcing caused by non-CO_2 effects is a complex process, leading to results that are affected by large uncertainties due to, for example, incomplete scientific understanding and modeling capabilities (Lee et al., 2021). As described in Sect. 3.1, we use the aCCFs version 1.0A to estimate the climate impact of aviation (Matthes et al., 2023b), which are calibrated towards the results of a climate response model (AirClim, Dahlmann et al., 2016) to align the relative importance of individual aCCFs. This is an update of the consistent set of aCCF 1.0 (Yin et al., 2023), calculating the climate impact of CO_2, H_2O, NO_x-ozone, NO_x-methane and contrails in terms of ATR20, assuming pulse emissions (P-ATR20). This prototype set of functions are the focus of on-going research, to address their sources of uncertainties. Moreover, we employed factors to: (1) convert the aCCFs values to a different climate metric, F-ATR20, which assumes a business-as-usual future emission scenario; (2) include the efficacy of each climate impact effect ~~(Dietmüller et al., 2022)~~ (Dietmüller et al., 2023). These assumptions introduce additional sources of uncertainties (Matthes et al., 2023a). Moreover, ~~we~~ the majority of ice-supersaturated regions (supporting persistent contrail formation) have characteristic dimensions that are smaller than the horizontal resolution of our model. To take this factor into account, we employ a parameterization developed by Burkhardt et al. (2008) to estimate the fraction of model grid box which is supporting persistent contrails. The potential of reducing the flights climate impact by contrail avoidance could be reduced by factors not included in this study. For example, here we use weather conditions simulated by an atmospheric model (EMAC) rather than weather forecast. In real life applications, this mitigation strategy relies on the accuracy and stability of weather forecast, as discussed in Sect. 1. Lastly, we note that we use a simplified representation of the operating cost, to limit the computational time required for their evaluation within each optimization step. To this end, we assume a linear relationship between cost of time and flight time (see Eq. (1) and Yamashita et al., 2020). Therefore, we neglect additional costs caused by delays. Further research will explore the impact of optimizing not only the location of the flight trajectory (see Sect. 2.2), but also the airspeed, improving fuel efficiency compared to this study, which assumed a constant Mach number for all solutions. Other studies found that speed changes can be important for reducing fuel flow, NO_x emissions and, ultimately, NO_x climate effects (Simorgh et al., 2023). This improvement of AirTraf is expected to impact the SolFinder results, by reducing the penalties in terms of operating costs and CO_2 emissions for a certain gain in terms of reduction of ATR20. On the other hand, including the airspace structure and capacity, which are neglected in this study, can reduce the estimated climate impact mitigation potential of this operational strategy.

5 Conclusions

In this study, we described the decision-making strategies implemented in the SolFinder 1.0 module. The SolFinder 1.0 module has been coupled to the AirTraf 3.0 submodel, as part of its development to efficiently solve multi-objective optimization problems. ~~AirTraf is coupled to an atmospheric chemistry model (EMAC): thus, using this modelling chain, we~~ We showed here how the selected decision-making strategies can be used to identify solutions matching specific preferences (e.g., eco-efficient aircraft trajectories)~~,~~. Moreover, using this modelling chain, it is possible to explore the results variability under

~~different weather patterns~~ a large number of consecutive days, due to the coupling between SolFinder and an atmospheric chemistry model (EMAC), via the EMAC submodel AirTraf. To demonstrate the usage of the tool, this paper showed results

470 for the period of one winter month (1-31 January 2018). We solved a bi-objective optimization problem minimizing the climate impact of the aircraft trajectory (F-ATR20$_{tot}$) and its simple operating costs (SOC), and we compared the solutions selected by different configurations of SolFinder 1.0. Comparing the strategies using VIKOR and a target change in SOC, we found that lower values of the climate-cost coefficient k [\$/K] (i.e., a higher eco-efficiency) are obtained with the former option. The ~~decision making~~ decision-making strategies included in SolFinder 1.0 are applied on sets of Pareto-optimal solutions relative

475 to a single aircraft trajectory. In the next SolFinder versions, we plan to take into account the mitigation potential variability across all flights. As a result, only the best performing fraction of the flights is optimized with respect to their climate impact, and the cost of the operational mitigation strategy is lowered. On-going research is using the modelling chain presented in this paper to identify those weather situations allowing for the largest reductions in the temperature response from aviation emissions via the optimization of aircraft trajectories.

480 *Code and data availability.* The Modular Earth Submodel System (MESSy) is continuously further developed and applied by a consortium of institutions. The usage of MESSy and access to the source code is licenced to all affiliates of institutions which are members of the MESSy Consortium. Institutions can become a member of the MESSy Consortium by signing the MESSy Memorandum of Understanding. More information can be found on the MESSy Consortium Website (http://www.messy-interface.org). The code presented here has been based on MESSy version 2.55.0 and will be available after the official release of AirTraf 3.0, a submodel of MESSy. An open access version

485 of SolFinder (see Supplement material) is available from the 4TU.ResearchData repository (Castino, 2023) under the licence GNU Lesser General Public License v3.0, as are the scripts to produce the plots presented in this paper. The simulation output analysed in this paper is archived in the 4TU.ResearchData repository (Castino et al., 2023).

Appendix A: VIKOR method

In this Sect. A, we quote the steps characterizing the VIKOR method, as they were introduced and described in Opricovic

490 (1998) and Opricovic and Tzeng (2004). Fig. A1 illustrates the main working principles of the VIKOR method. The x-axis represents the normalized distance from the minimum value of f_1, scaled by its relative weight w_1. As an example, this weight is set to $w_1 = 0.2$, thus the x-axis ranges from 0 to 0.2. Similarly, the y-axis represents the normalized distance from the minimum value of f_2, weighted using $w_2 = 0.8$. The axes intersect at the reference point i_{best}, defined as the best *ideal* (i.e., usually not feasible) solution. Opposite to i_{best}, it is possible to identify i_{worst}, which assumes the worst values of f_n ($f_{n,worst}$) found among

495 the set of Pareto-optimal solutions. For example, when aiming at minimizing f_n, i_{worst} corresponds to the maximum f_n among the Pareto set. The grey points in Fig. A1 indicate the location of the Pareto-optimal solutions, relative to i_{best}. In ~~facts~~ fact, the VIKOR method ranks the Pareto-optimal solutions using ~~as reference point i_{best}~~ i_{best} as a reference point. Hence, the first step consists ~~in identifying such~~ of identifying such a reference point, by determining the best values of each of the objectives, $f_{n,best}$. Since we aim to minimize the objective functions, we use the following definitions of $f_{n,best}$ and $f_{n,worst}$:

$$500 \quad f_{n,\text{best}} = \min_{j} f_{n,j}, \qquad f_{n,\text{worst}} = \max_{j} f_{n,j}, \qquad n = 1, 2, ..., N, \qquad j = 1, 2, ..., J \tag{A1}$$

In Fig. A1 we highlight the Pareto-optimal solution p_j. In the second step of the VIKOR method, two quantities are calculated for each point in the Pareto set: $S(p_j)$, which measures the *group utility* of the solution p_j, and $R(p_j)$, which represents its *individual regret*. In other words, $S(p_j)$ measures the overall distance of p_j from i_{best}, taking into account all the optimization objectives. On the other hand, $R(p_j)$ measures the largest distance of p_j from i_{best} considering each objective individually. These quantities are defined by Eqs. (4) and (5), respectively:

$$S(p_j) = \sum_{n=1}^{N} w_n \frac{f_{n,\text{best}} - f_{n,j}}{f_{n,\text{best}} - f_{n,\text{worst}}} \tag{A2}$$

$$R(p_j) = \max_{n} \left[w_n \frac{f_{n,\text{best}} - f_{n,j}}{f_{n,\text{best}} - f_{n,\text{worst}}} \right] \tag{A3}$$

where w_n is the relative weight of each objective f_n.

The geometric representation of $S(p_j)$ and $R(p_j)$ is illustrated in Fig. A1. It is possible to deduce from Eqs. (4) and (5) and from Fig. A1 that lower values of $S(p_j)$ and $R(p_j)$ are preferable. These measures of the distance of p_j from i_{best} are combined in the value $Q(p_j)$, which is used as main ranking parameter by the VIKOR method. The value of $Q(p_j)$ is calculated using Eq. (6):

$$Q(p_j) = \gamma \frac{S_j - \min_j S_j}{\max_j S_j - \min_j S_j} + (1 - \gamma) \frac{R_j - \min_j R_j}{\max_j R_j - \min_j R_j} \tag{A4}$$

The next step consists in creating three ranking lists of the ~~Pareto optimal~~ Pareto-optimal solutions, sorting them by S, R, and Q. We define p_i as the Pareto-optimal solution at the ith position in the list sorted by Q. Consequently, the first compromise solution to be recommended is p_1, which minimizes Q: $Q(p_1) = \min_j Q(p_j)$. The following conditions are then evaluated:

1. **acceptable advantage**: $Q(p_2) - Q(p_1) \geq \frac{1}{J-1}$

   If this condition is not verified, a set of Pareto-optimal solutions p_v $(v = 1, 2, ..., M)$ is recommended, where M is the maximum value for which $Q(p_M) - Q(p_1) \leq \frac{1}{J-1}$ is true.

2. **acceptable stability**: p_1 is the best ranked solution not only by Q, but also by S and R.

   If this condition is not satisfied, both p_1 and p_2 are recommended.

Therefore, the application of the VIKOR method results in the identification of either one optimal solution, p_1, or a subset of optimal solutions, p_v $(v = 1, 2, ..., M)$, which are recommended to the decision-maker.
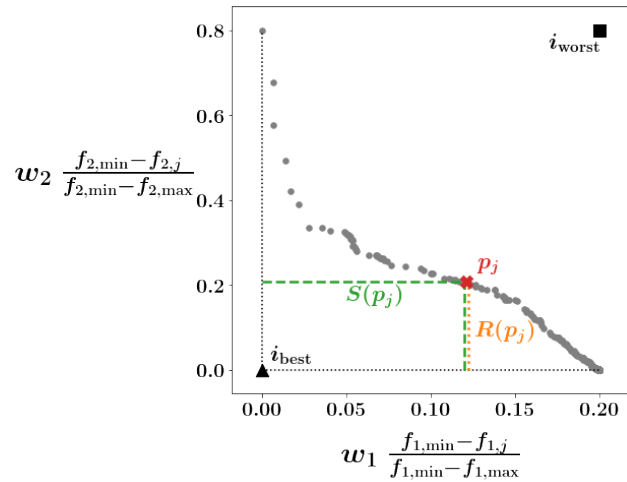
Figure A1. Illustration of the VIKOR method applied to a bi-objective optimization problem, minimizing f_1 and f_2. In this example, we set $w_1 = 0.2$ and $w_2 = 0.8$, thus the x (y) axis ranges from 0.0 to 0.2 (0.8). The grey dots represent Pareto-optimal solutions. The red cross indicates the Pareto-optimal solution p_j. The green dashed line represents $S(p_j)$, while the orange dotted segment represents $R(p_j)$. The reference points i_{best} and i_{worst} are indicated by the black triangle and black square, respectively.

Appendix B: Air traffic sample

	ICAO airport code			ICAO airport code	
citypairs	departure	arrival	citypairs	departure	arrival
0	LTFM	EGLL	50	EDDL	LTFM
1	EGLL	LTFM	51	LTFM	EDDL
2	LEMD	GCLP	52	LFPO	LFBO
3	GCLP	LEMD	53	LEMD	EHAM
4	GCXO	LEMD	54	LFBO	LFPO
5	LEMD	GCXO	55	EHAM	LEMD
6	LFPG	LTFM	56	LFMN	LFPO
7	LTFM	LFPG	57	LFPO	LFMN
8	EGLL	LEMD	58	EGLL	LPPT
9	LFPO	LPPT	59	LPPT	EGLL
10	LPPT	LFPO	60	LEBL	LEMD
11	LEMD	EGLL	61	LFPG	LIRF
12	LEPA	EDDL	62	LIRF	LFPG
13	EDDL	LEPA	63	EHAM	LIRF
14	EHAM	LTFM	64	LIRF	EHAM
15	LTFM	EHAM	65	LEPA	EDDT
16	LGAV	EGLL	66	EDDT	LEPA
17	EGLL	LGAV	67	LEMD	LFPO
18	LEBL	EGKK	68	LFPO	LEMD
19	EGKK	LEBL	69	EDDM	EGLL
20	LEMD	LIRF	70	EGLL	EDDM
21	LIRF	LEMD	71	LEMD	LEBL
22	ESSA	EGLL	72	UBBB	LTFM
23	EGLL	ESSA	73	LTCG	LTFJ
24	EHAM	LEBL	74	LTFJ	LTCG
25	LEBL	EHAM	75	LFPG	LGAV
26	EDDF	LEMD	76	LGAV	LFPG
27	EGCC	GCTS	77	LEMD	EDDM
28	LEMD	EDDF	78	EDDM	LEMD
29	GCTS	EGCC	79	ESSA	LEMG
30	LPPT	EDDF	80	LEMG	ESSA
31	EDDF	LPPT	81	LEMD	EBBR
32	LIRF	EGLL	82	EBBR	LEMD
33	EGLL	LIRF	83	LROP	EGGW
34	LPPT	EHAM	84	EGGW	LROP
35	EHAM	LPPT	85	LPPT	EBBR
36	ENGM	ENTC	86	LTFM	UBBB
37	LTFM	EDDF	87	EBBR	LPPT
38	EDDF	LTFM	88	LEMG	EFHK
39	EGKK	LEMG	89	EFHK	LEMG
40	ENTC	ENGM	90	GCXO	LEBL
41	LEMG	EGKK	91	LEBL	GCXO
42	EGLL	EFHK	92	LTAI	EDDK
43	EFHK	EGLL	93	EDDK	LEPA
44	LTAI	EDDL	94	LEPA	EDDK
45	EDDL	LTAI	95	EDDH	LEPA
46	GCTS	EGKK	96	EDDT	EDDF
47	EGKK	GCTS	97	LEPA	EDDH
48	LEMG	EKCH	98	EDDF	EDDT
49	EKCH	LEMG	99	LPPR	LFPO

Figure B1. List of origin/destination airport pairs included in the air traffic sample, as illustrated in the map in Fig. 5.

525 *Author contributions.* FC, FY, VG, and HY developed the concepts presented in this paper. FC and HY implemented the decision-making module in the AirTraf submodel. FC performed the simulations and analysed the results presented in this paper. SM and SD provided the aCCFs formulas and factors employed in this study. BL, FL, and MMM provided the air traffic sample employed this study. All co-authors contributed to the discussion and the revision of the paper.

Competing interests. At least one of the (co-)authors is a member of the editorial board of Geoscientific Model Development. The peer-
530 review process was guided by an independent editor, and the authors also have no other competing interests to declare.

Acknowledgements. The current study has been supported by FlyATM4E project, which has received funding from the SESAR Joint Under-taking (JU) under grant agreement No 891317. The JU receives support from the European Union's Horizon 2020 research and innovation programme and the SESAR JU members other than the Union. The computing resources to conduct simulations with the ECHAM/MESSy Atmospheric Chemistry (EMAC) model were provided by the TU Delft High Performance Cluster (HPC12).

535 References

Burkhardt, U., Kärcher, B., Ponater, M., Gierens, K., and Gettelman, A.: Contrail cirrus supporting areas in model and observations, Geophysical Research Letters, 35, https://doi.org/10.1029/2008GL034056, 2008.

Burris, M. A.: Cost index estimation, in: IATA 3rd Airline Cost Conference, Geneva, Switzerland, p. 1–23, 2015.

Castino, F.: Code accompanying the manuscript "Decision-Making strategies implemented in SolFinder 1.0 to identify eco-efficient aircraft
540   trajectories: application study in AirTraf 3.0", 4TU.ResearchData, https://doi.org/10.4121/3744b922-ffa6-4f92-ad57-dc93f94e969b, 2023.

Castino, F., Yin, F., Grewe, V., Soler, M., Simorgh, A., Yamashita, H., Matthes, S., Baumann, S., Dietmüller, S., Linke, F., and Lührs, B.: Seasonal Variability of Aircraft Trajectories reducing NOx-climate Impacts under a Multitude of Weather Patterns, 11th SESAR Innovation Days, 2021.

Castino, F., Yin, F., and Yamashita, H.: Data accompanying the manuscript "Decision-Making strategies implemented in SolFinder 1.0 to
545   identify eco-efficient aircraft trajectories: application study in AirTraf 3.0", 4TU.ResearchData, https://doi.org/10.4121/57b96974-6ec7-4e86-9d95-2b7bf3c18d8f, 2023.

Chen, S.-J. and Hwang, C.-L.: Fuzzy Multiple Attribute Decision Making, vol. 375, Springer Berlin Heidelberg, Berlin, Heidelberg, https://doi.org/10.1007/978-3-642-46768-4, 1992.

Dahlmann, K., Grewe, V., Frömming, C., and Burkhardt, U.: Can we reliably assess climate mitigation options for air traffic scenar-
550   ios despite large uncertainties in atmospheric processes?, Transportation Research Part D: Transport and Environment, 46, 40–55, https://doi.org/10.1016/j.trd.2016.03.006, 2016.

Dee, D. P., Uppala, S. M., Simmons, A. J., Berrisford, P., Poli, P., Kobayashi, S., Andrae, U., Balmaseda, M. A., Balsamo, G., Bauer, P., Bechtold, P., Beljaars, A. C. M., van de Berg, L., Bidlot, J., Bormann, N., Delsol, C., Dragani, R., Fuentes, M., Geer, A. J., Haimberger, L., Healy, S. B., Hersbach, H., Hólm, E. V., Isaksen, L., Kållberg, P., Köhler, M., Matricardi, M., McNally, A. P., Monge-Sanz,
555   B. M., Morcrette, J.-J., Park, B.-K., Peubey, C., de Rosnay, P., Tavolato, C., Thépaut, J.-N., and Vitart, F.: The ERA-Interim reanalysis: configuration and performance of the data assimilation system, Quarterly Journal of the Royal Meteorological Society, 137, 553–597, https://doi.org/10.1002/qj.828, 2011.

Dietmüller, S., Matthes, S., Dahlmann, K., Yamashita, H., Simorgh, A., Soler, M., Linke, F., Lührs, B., Mendiguchia Meuser, M., Weder, C., Grewe, V., Yin, F., and Castino, F.: A python library for computing individual and merged non-CO2 algorithmic climate change functions:
560   CLIMaCCF V1.0, Geosci. Model Dev. Discuss. [preprint], https://doi.org/10.5194/gmd-2022-203, 2022.

Dietmüller, S., Matthes, S., Dahlmann, K., Yamashita, H., Simorgh, A., Soler, M., Linke, F., Lührs, B., Meuser, M. M., Weder, C., Grewe, V., Yin, F., and Castino, F.: A Python library for computing individual and merged non-CO2 algorithmic climate change functions: CLIMaCCF V1.0, Geoscientific Model Development, 16, 4405–4425, https://doi.org/10.5194/gmd-16-4405-2023, 2023.

Eurocontrol: User Manual for the Base of Aircraft Data (BADA) Revision 3.9, EEC Technical/Scientific Report No.12/04/10-45, Tech. rep.,
565   2011.

Frömming, C., Ponater, M., Dahlmann, K., Grewe, V., Lee, D. S., and Sausen, R.: Aviation-induced radiative forcing and surface temperature change in dependency of the emission altitude, Journal of Geophysical Research Atmospheres, 117, 1–15, https://doi.org/10.1029/2012JD018204, 2012.

Frömming, C., Grewe, V., Brinkop, S., and Jöckel, P.: Documentation of the EMAC submodels AIRTRAC 1.0 and CONTRAIL 1.0, sup-
570   plementary material of Grewe et al., 2014, 7, 175–201, Geoscientific Model Development, https://doi.org/10.5194/gmd-7-175-2014%0A, 2014.

Frömming, C., Grewe, V., Brinkop, S., Jöckel, P., Haslerud, A. S., Rosanka, S., Van Manen, J., and Matthes, S.: Influence of weather situation on non-CO2 aviation climate effects: The REACT4C climate change functions, Atmospheric Chemistry and Physics, 21, 9151–9172, https://doi.org/10.5194/acp-21-9151-2021, 2021.

575 Grewe, V., Matthes, S., Frömming, C., Brinkop, S., Jöckel, P., Gierens, K., Champougny, T., Fuglestvedt, J., Haslerud, A., Irvine, E., and Shine, K.: Feasibility of climate-optimized air traffic routing for trans-Atlantic flights, Environmental Research Letters, 12, https://doi.org/10.1088/1748-9326/aa5ba0, 2017.

Jöckel, P., Kerkweg, A., Pozzer, A., Sander, R., Tost, H., Riede, H., Baumgaertner, A., Gromov, S., and Kern, B.: Development cycle 2 of the Modular Earth Submodel System (MESSy2), Geoscientific Model Development, 3, 717–752, https://doi.org/10.5194/gmd-3-717-2010, 580 2010.

Jöckel, P., Tost, H., Pozzer, A., Kunze, M., Kirner, O., Brenninkmeijer, C. A. M., Brinkop, S., Cai, D. S., Dyroff, C., Eckstein, J., Frank, F., Garny, H., Gottschaldt, K.-D., Graf, P., Grewe, V., Kerkweg, A., Kern, B., Matthes, S., Mertens, M., Meul, S., Neumaier, M., Nützel, M., Oberländer-Hayn, S., Ruhnke, R., Runde, T., Sander, R., Scharffe, D., and Zahn, A.: Earth System Chemistry integrated Mod- elling (ESCiMo) with the Modular Earth Submodel System (MESSy) version 2.51, Geoscientific Model Development, 9, 1153–1200, 585 https://doi.org/10.5194/gmd-9-1153-2016, 2016.

Kärcher, B.: Formation and radiative forcing of contrail cirrus, Nature Communications, 9, 1824, https://doi.org/10.1038/s41467-018-04068- 0, 2018.

Köhler, M. O., Rädel, G., Dessens, O., Shine, K. P., Rogers, H. L., Wild, O., and Pyle, J. A.: Impact of perturbations to nitrogen oxide emissions from global aviation, Journal of Geophysical Research Atmospheres, 113, 1–15, https://doi.org/10.1029/2007JD009140, 2008.

590 Köhler, M. O., Rädel, G., Shine, K. P., Rogers, H. L., and Pyle, J. A.: Latitudinal variation of the effect of avia- tion NOx emissions on atmospheric ozone and methane and related climate metrics, Atmospheric Environment, 64, 1–9, https://doi.org/10.1016/j.atmosenv.2012.09.013, 2013.

Kou, G., Lu, Y., Peng, Y., and Shi, Y.: Evaluation of classification algorithms using MCDM and rank correlation, International Journal of Information Technology and Decision Making, 11, 197–225, https://doi.org/10.1142/S0219622012500095, 2012.

595 Lee, D. S., Pitari, G., Grewe, V., Gierens, K., Penner, J. E., Petzold, A., Prather, M. J., Schumann, U., Bais, A., Berntsen, T., Iachetti, D., Lim, L. L., and Sausen, R.: Transport impacts on atmosphere and climate: Aviation, Atmospheric Environment, 44, 4678–4734, https://doi.org/10.1016/j.atmosenv.2009.06.005, 2010.

Lee, D. S., Fahey, D. W., Skowron, A., Allen, M. R., Burkhardt, U., Chen, Q., Doherty, S. J., Freeman, S., Forster, P. M., Fuglestvedt, J., Gettelman, A., De León, R. R., Lim, L. L., Lund, M. T., Millar, R. J., Owen, B., Penner, J. E., Pitari, G., Prather, M. J., Sausen, R., and 600 Wilcox, L. J.: The contribution of global aviation to anthropogenic climate forcing for 2000 to 2018, Atmospheric Environment, 244, https://doi.org/10.1016/j.atmosenv.2020.117834, 2021.

Lührs, B., Linke, F., Matthes, S., Grewe, V., and Yin, F.: Climate impact mitigation potential of European air traffic in a weather situation with strong contrail formation, Aerospace, 8, 1–15, https://doi.org/10.3390/aerospace8020050, 2021.

Matthes, S., Grewe, V., Dahlmann, K., Frömming, C., Irvine, E., Lim, L., Linke, F., Lührs, B., Owen, B., Shine, K., Stromatas, 605 S., Yamashita, H., and Yin, F.: A concept for multi-criteria environmental assessment of aircraft trajectories, Aerospace, 4, https://doi.org/10.3390/aerospace4030042, 2017.

Matthes, S., Lührs, B., Dahlmann, K., Grewe, V., Linke, F., Yin, F., Klingaman, E., and Shine, K. P.: Climate-optimized trajectories and robust mitigation potential: Flying atm4e, Aerospace, 7, 1–15, https://doi.org/10.3390/aerospace7110156, 2020.

Matthes, S., Lim, L., Burkhardt, U., Dahlmann, K., Dietmüller, S., Grewe, V., Haslerud, A. S., Hendricks, J., Owen, B., Pitari, G., Righi, M., and Skowron, A.: Mitigation of Non-CO2 Aviation's Climate Impact by Changing Cruise Altitudes, Aerospace, 8, 1–20, https://doi.org/10.3390/aerospace8020036, 2021.

Matthes, S., Dahlmann, K., Dietmüller, S., Yamashita, H., Baumann, S., Soler, M., Simorgh, A., González Arriba, D., Linke, F., Lührs, B., Meuser, M., Castino, F., and Yin, F.: How to integrate uncertainties when identifying robust climate-optimized aircraft trajectories in FlyATM4E, Contributions to Atmospheric Sciences, In Preparation, 2023a.

Matthes, S., Dietmüller, S., Dahlmann, K., Frömming, C., Peter, P., Yamashita, H., Grewe, V., Yin, F., and Castino, F.: Updated algorithmic climate change functions (aCCF) V1.0A: Evaluation with the climate-response model AirClim V2.0, Geosci. Model Dev. Discuss. [preprint], https://doi.org/10.5194/gmd-2023-92, 2023b.

Molloy, J., Teoh, R., Harty, S., Koudis, G., Schumann, U., Poll, I., and Stettler, M. E. J.: Design Principles for a Contrail-Minimizing Trial in the North Atlantic, Aerospace, 9, 375, https://doi.org/10.3390/aerospace9070375, 2022.

Opricovic, S.: Multicriteria Optimization of Civil Engineering Systems, Ph.D. thesis, University of Belgrade, Belgrade, 1998.

Opricovic, S. and Tzeng, G.-H.: Compromise solution by MCDM methods: A comparative analysis of VIKOR and TOPSIS, European Journal of Operational Research, 156, 445–455, https://doi.org/10.1016/S0377-2217(03)00020-1, 2004.

Pasman, H. J., Rogers, W. J., and Behie, S. W.: Selecting a method/tool for risk-based decision making in complex situations, Journal of Loss Prevention in the Process Industries, 74, https://doi.org/10.1016/j.jlp.2021.104669, 2022.

Reutter, P., Neis, P., Rohs, S., and Sauvage, B.: Ice supersaturated regions: properties and validation of ERA-Interim reanalysis with IAGOS in situ water vapour measurements, Atmospheric Chemistry and Physics, 20, 787–804, https://doi.org/10.5194/acp-20-787-2020, 2020.

Roeckner, E., Brokopf, R., Esch, M., Giorgetta, M. A., Hagemann, S., Kornblueh, L., Manzini, E., Schlese, U., and Schulzweida, U.: Sensitivity of simulated climate to horizontal and vertical resolution in the ECHAM5 atmosphere model, Journal of Climate, 19, 3771–3791, https://doi.org/10.1175/JCLI3824.1, 2006.

Sałabun, W., Wątróbski, J., and Shekhovtsov, A.: Are MCDA Methods Benchmarkable? A Comparative Study of TOPSIS, VIKOR, CO-PRAS, and PROMETHEE II Methods, Symmetry, 12, 1549, https://doi.org/10.3390/sym12091549, 2020.

Sasaki, D. and Obayashi, S.: Efficient search for trade-offs by adaptive range multi-objective genetic algorithms, Journal of Aerospace Computing, Information and Communication, 2, 44–64, https://doi.org/10.2514/1.12909, 2005.

Schumann, U.: Formation, properties and climatic effects of contrails, Comptes Rendus Physique, 6, 549–565, https://doi.org/10.1016/j.crhy.2005.05.002, 2005.

Simorgh, A., Soler, M., González-Arribas, D., Matthes, S., Grewe, V., Dietmüller, S., Baumann, S., Yamashita, H., Yin, F., Castino, F., Linke, F., Lührs, B., and Meuser, M. M.: A Comprehensive Survey on Climate Optimal Aircraft Trajectory Planning, https://doi.org/10.3390/aerospace9030146, 2022.

Simorgh, A., Soler, M., González-Arribas, D., Linke, F., Lührs, B., Meuser, M. M., Dietmüller, S., Matthes, S., Yamashita, H., Yin, F., Castino, F., Grewe, V., and Baumann, S.: Robust 4D climate-optimal flight planning in structured airspace using parallelized simulation on GPUs: ROOST V1.0, Geoscientific Model Development, 16, 3723–3748, https://doi.org/10.5194/gmd-16-3723-2023, 2023.

Sridhar, B., Ng, H. K., and Chen, N. Y.: Aircraft Trajectory Optimization and Contrails Avoidance in the Presence of Winds, Journal of Guidance, Control, and Dynamics, 34, 1577–1584, https://doi.org/10.2514/1.53378, 2011.

Staples, M. D., Malina, R., Suresh, P., Hileman, J. I., and Barrett, S. R.: Aviation CO2 emissions reductions from the use of alternative jet fuels, Energy Policy, 114, 342–354, https://doi.org/10.1016/j.enpol.2017.12.007, 2018.

Stevenson, D. S. and Derwent, R. G.: Does the location of aircraft nitrogen oxide emissions affect their climate impact?, Geophysical Research Letters, 36, 4–8, https://doi.org/10.1029/2009GL039422, 2009.

Stevenson, D. S., Doherty, R. M., Sanderson, M. G., Collins, W. J., Johnson, C. E., and Derwent, R. G.: Radiative forcing from aircraft NOx emissions: Mechanisms and seasonal dependence, Journal of Geophysical Research D: Atmospheres, 109, https://doi.org/10.1029/2004JD004759, 2004.

650

van Manen, J. and Grewe, V.: Algorithmic climate change functions for the use in eco-efficient flight planning, Transportation Research Part D: Transport and Environment, 67, 388–405, https://doi.org/10.1016/j.trd.2018.12.016, 2019.

Wang, Z. and Rangaiah, G. P.: Application and Analysis of Methods for Selecting an Optimal Solution from the Pareto-Optimal Front obtained by Multiobjective Optimization, Industrial & Engineering Chemistry Research, 56, 560–574, https://doi.org/10.1021/acs.iecr.6b03453, 2017.

655

Yamashita, H., Grewe, V., Jöckel, P., Linke, F., Schaefer, M., and Sasaki, D.: Air traffic simulation in chemistry-climate model EMAC 2.41: AirTraf 1.0, Geoscientific Model Development, 9, 3363–3392, https://doi.org/10.5194/gmd-9-3363-2016, 2016.

Yamashita, H., Yin, F., Grewe, V., Jöckel, P., Matthes, S., Kern, B., Dahlmann, K., and Frömming, C.: Newly developed aircraft routing options for air traffic simulation in the chemistry–climate model EMAC 2.53: AirTraf 2.0, Geoscientific Model Development, 13, 4869–4890, https://doi.org/10.5194/gmd-13-4869-2020, 2020.

660

Yamashita, H., Yin, F., Grewe, V., Jöckel, P., Matthes, S., Kern, B., Dahlmann, K., and Frömming, C.: Analysis of aircraft routing strategies for north atlantic flights by using airtraf 2.0, Aerospace, 8, 1–19, https://doi.org/10.3390/aerospace8020033, 2021.

Yin, F. and Rao, A. G.: A review of gas turbine engine with inter-stage turbine burner, Progress in Aerospace Sciences, 121, 100 695, https://doi.org/10.1016/j.paerosci.2020.100695, 2020.

665

Yin, F., Grewe, V., Castino, F., Rao, P., Matthes, S., Dahlmann, K., Dietmüller, S., Frömming, C., Yamashita, H., Peter, P., Klingaman, E., Shine, K. P., Lührs, B., and Linke, F.: Predicting the climate impact of aviation for en-route emissions: the algorithmic climate change function submodel ACCF 1.0 of EMAC 2.53, Geoscientific Model Development, 16, 3313–3334, https://doi.org/10.5194/gmd-16-3313-2023, 2023.

Table 3. Properties of the trajectories selected within the 1st set of experiments. The table provides the total monthly percentage changes in climate impact, ΔATR20$_{tot}$ [%], in simple operating cost, ΔSOC [%], in fuel used, ΔFuel [%], and in flight time, ΔTime [%], relative to the respective total values from the cost-optimal scenario; and values of the climate-cost coefficient k [$/K]. The minimum and maximum daily values are included within brackets.

SolFinder Strategy	ΔATR20 [%]	ΔSOC [%]	ΔFuel [%]	ΔTime [%]	Coeff. k [$/K]
Climate-optimal	-14.4(-29.2, -6.7)	+3.04(+1.32, +5.00)	+8.14(+2.41,+15.19)	+1.01(+0.59, +1.52)	3.95e+12(1.58e+12, 1.33e+13)
VIKOR w_{SOC}=0.2	-12.8(-26.0, -5.9)	+2.00(+0.72, +3.52)	+5.72(+1.38,+11.18)	+0.51(+0.07, +0.98)	2.94e+12(1.07e+12, 1.05e+13)
VIKOR w_{SOC}=0.4	-10.3(-21.1, -4.7)	+1.19(+0.42, +2.56)	+3.50(+0.70, +8.28)	+0.27(+0.01, +0.57)	2.21e+12(6.05e+11, 9.37e+12)
VIKOR w_{SOC}=0.6	-7.9(-13.8, -4.0)	+0.67(+0.21, +1.52)	+1.86(+0.30, +5.07)	+0.20(-0.01, +0.34)	1.66e+12(4.65e+11, 8.10e+12)
VIKOR w_{SOC}=0.7	-6.2(-11.0, -2.8)	+0.40(+0.14, +0.74)	+1.09(+0.19, +2.61)	+0.12(-0.04, +0.27)	1.27e+12(3.71e+11, 6.54e+12)
VIKOR w_{SOC}=0.8	-4.9(-8.7, -1.3)	+0.22(+0.09, +0.34)	+0.55(+0.05, +1.30)	+0.08(-0.09, +0.22)	8.81e+11(2.37e+11, 4.31e+12)
VIKOR w_{SOC}=0.9	-3.5(-6.3, -0.5)	+0.11(+0.06, +0.18)	+0.25(-0.00, +0.46)	+0.06(-0.05, +0.16)	6.46e+11(1.80e+11, 2.85e+12)

Table 4. Properties of the trajectories selected within the 2nd set of experiments. The table provides the total monthly percentage changes in climate impact, ΔATR20 [%], in simple operating cost, ΔSOC [%], in fuel used, ΔFuel [%], and in flight time, ΔTime [%], relative to the respective total values of the cost-optimal scenario; and values of the climate-cost coefficient k [$/K]. The minimum and maximum daily values are included within brackets.

SolFinder Strategy	ΔATR20 [%]	ΔSOC [%]	ΔFuel [%]	ΔTime [%]	Coeff. k [$/K]
+3.0% SOC	-12.5(-25.2, -6.3)	+1.92(+1.00, +2.82)	+5.47(+1.79, +9.55)	+0.51(-0.05, +0.91)	2.90e+12(1.22e+12, 9.67e+12)
+2.0% SOC	-11.1(-21.5, -5.7)	+1.43(+0.82, +1.96)	+4.04(+1.34, +6.94)	+0.39(-0.11, +0.72)	2.44e+12(9.40e+11, 8.45e+12)
+1.0% SOC	-8.7(-14.9, -3.4)	+0.80(+0.59, +0.98)	+2.14(+0.82, +3.59)	+0.26(-0.13, +0.52)	1.79e+12(6.72e+11, 7.08e+12)
+0.5% SOC	-6.9(-12.8, -2.0)	+0.42(+0.36, +0.50)	+1.02(+0.39, +1.90)	+0.19(-0.06, +0.36)	1.27e+12(3.89e+11, 6.13e+12)
VIKOR w=0.7, +1.0% SOC	-6.0(-10.7, -2.4)	+0.35(+0.14, +0.61)	+0.94(+0.19, +2.21)	+0.11(-0.05, +0.24)	1.18e+12(3.52e+11, 6.38e+12)